

Stellar Populations of Dwarf Elliptical Galaxies: UBVRI Photometry of Dwarf Elliptical Galaxies in the Virgo Cluster ¹

Liese van Zee

Astronomy Department, Indiana University, 727 E 3rd St., Bloomington, IN 47405

vanzee@astro.indiana.edu

Elizabeth J. Barton²

Steward Observatory, University of Arizona, 933 N Cherry St., Tucson, AZ 85721

ebarton@as.arizona.edu

and

Evan D. Skillman

Astronomy Department, University of Minnesota, 116 Church St. SE, Minneapolis, MN 55455

skillman@astro.umn.edu

ABSTRACT

We present UBVRI surface photometry for 16 dwarf elliptical galaxies in the Virgo Cluster with previously measured kinematic properties. The global optical colors are red, with median values for the sample of 0.24 ± 0.03 in (U–B), 0.77 ± 0.02 in (B–V), and 1.02 ± 0.03 in (V–I). We recover the well known color-magnitude relation for cluster galaxies, but find no significant difference in dominant stellar population between rotating and non-rotating dwarf elliptical galaxies; the average age of the dominant stellar population is 5–7 Gyr in all 16 galaxies in this sample. Analysis of optical spectra confirm these age estimates and indicate Fe and Mg abundances in the range of 1/20th to 1/3 of solar, as expected for low luminosity galaxies. Based on Lick indices and simple stellar population models, the derived $[\alpha/\text{Fe}]$ ratios are sub-solar to solar, indicating a more gradual chemical enrichment history for dEs as compared to giant elliptical galaxies in the Virgo Cluster. These observations confirm the marked difference in stellar population and stellar distribution between dwarf and giant elliptical galaxies and further substantiate the need for alternative evolutionary scenarios for the lowest mass cluster galaxies. We argue that it is likely that several different physical mechanisms played a significant role in the production of the Virgo cluster dE galaxies including *in situ* formation, infall of dEs that were once part of Local Group analogs, and transformation of dwarf irregular galaxies by the cluster environment. The observations support the hypothesis that a large fraction of the Virgo cluster dEs are formed by ram pressure stripping of gas from infalling dIs.

Subject headings: galaxies: clusters: general — galaxies: dwarf — galaxies: evolution
— galaxies: fundamental parameters — galaxies: photometry

1. Introduction

Dwarf elliptical galaxies are ubiquitous in high density regions. For example, in the Local Group, dwarf elliptical galaxies outnumber high luminosity galaxies by a factor of 6 (Mateo 1998), and more than 50% of the galaxies in the Virgo cluster are dEs (Sandage, Binggeli, & Tammann 1985). However, while the clustering properties of dwarf elliptical galaxies appear to be an extension of the well known morphology-density relation for giant elliptical galaxies (e.g., Dressler 1980; Postman & Geller 1984), their structural parameters suggest that dwarf ellipticals are not merely low mass versions of elliptical galaxies (e.g., Lin & Faber 1983; Kormendy 1985; Ichikawa, Wakamatsu, & Okamura 1986; Caldwell & Bothun 1987; Binggeli & Cameron 1991). Unlike their giant counterparts, gas-poor dwarf elliptical galaxies and gas-rich dwarf irregular galaxies have similar stellar distributions which suggests that passive evolution of the stellar population could result in morphological evolution from one dwarf classification to the other (e.g., Lin & Faber 1983; Kormendy 1985; Davies & Phillipps 1988). In fact, many of the key morphological differences between dwarf elliptical and dwarf irregular galaxies can be traced to the cessation of star formation activity rather than to dynamical differences between the two classes. In support of this, Skillman et al. (2003) note that the star formation histories of dwarf elliptical galaxies may be very similar to those of dwarf irregular galaxies right up to the point of the loss of their gas. These similarities led to the hypothesis that dwarf elliptical galaxies are evolved versions of dIs whose ISM has been disrupted by either internal (e.g., blow-out, Dekel & Silk 1986) or external (e.g., ram pressure stripping, Lin & Faber 1983) processes. In addition to similar stellar distributions, recent kinematic studies of dEs in the Virgo cluster indicate that a large fraction of dEs and dS0s have a significant rotational component (Pedraz et al. 2002; Geha et al. 2003; van Zee et al. 2004). Furthermore, the amplitudes of the dE rotation curves are comparable to those of similar luminosity dwarf irregular galaxies (van Zee et al. 2004). These results support the possibility that some cluster dEs are evolved dwarf irregular galaxies which have lost their ISM and thus have little-to-no star formation activity at the present epoch.

The possibility that some dIs evolve into dEs is almost tautological since dEs must have been gas-rich, star forming low mass galaxies at some point in the past. Thus, the key question for dwarf galaxy evolution is not *whether* dEs evolve from dIs, but, rather, *when* and *why* do some dwarf irregular galaxies lose their ISM and stop forming stars. The strong clustering properties

¹Based on observations with the VATT: the Alice P. Lennon Telescope and the Thomas J. Bannan Astrophysics Facility.

²Hubble Fellow

of dEs (e.g., Binggeli, Tarenghi, & Sandage 1990) suggest that environmental influences may play a key role in the gas-loss process. Possible evolution mechanisms include triggered bursts of star formation with subsequent blow-out of the ISM (e.g., Dekel & Silk 1986), or ram pressure stripping of the ISM as the galaxy plunges through the hot intra-cluster gas (e.g., Lin & Faber 1983). Both of these scenarios will result in an overabundance of dwarf elliptical galaxies in high density regions, but the resulting star formation histories are quite different. In a triggered starburst scenario, most of the star formation activity will take place in discrete events which may be correlated with passage through the cluster. On the other hand, if the ISM is lost through ram pressure stripping, most of the star formation activity will take place prior to the passage through the cluster, and may occur in a more quiescent manner, typical of dIs (van Zee 2001). Thus, examination of the stellar populations and relative chemical enrichments in dwarf elliptical galaxies may provide insight into which of these mechanisms is the dominant process for the evolution of dIs to dEs in high density regions.

Within the Local Supercluster, the Virgo cluster is the nearest high density region and thus provides an excellent environment in which to explore stellar populations and kinematic properties of low luminosity galaxies. At the same time, Virgo is dynamically young (e.g., Tully & Shaya 1984) and contains several substructural units (Binggeli et al. 1987); thus, with a well selected sample it may be possible to study the evolution of dwarf elliptical galaxies within the cluster itself. Recent observations of surface brightness fluctuations (Jerjen et al. 2004) have shown that the dE population is stretched in depth similarly to the bright elliptical population (Neilsen & Tsvetanov 2000; West & Blakeslee 2000) but not as extended as claimed previously by Young & Currie (1995). Furthermore, nucleated dEs appear to be more strongly clustered than non-nucleated dEs in the cluster (e.g., Binggeli et al. 1987). In this paper, we examine broad band optical colors and optical spectroscopy of 16 dwarf elliptical galaxies in the Virgo Cluster to investigate their star formation histories and to search for correlations between kinematic properties and past star formation activity. The sixteen galaxies in this sample were selected as part of a kinematic study of dwarf elliptical galaxies in Virgo (van Zee et al. 2004); approximately half of the sample have a significant rotational component.

As discussed in van Zee et al. (2004), it is likely that the rotating dwarf elliptical galaxies are remnants of dIs that have been stripped of their gas; the rotating dwarf elliptical galaxies tend to be located near the outskirts of the cluster and their rotation curves and maximum amplitude velocities are comparable to similar luminosity dwarf irregular galaxies. At the same time, the origin of the non-rotating dwarf ellipticals is unclear. Are these low luminosity galaxies which began with little-to-no angular momentum? Were they formed through the collision of even lower mass galaxies and thus ended up with no net angular momentum? Did they transfer their angular momentum as they moved through the dense cluster? In support of the latter process, Mayer et al. (2001a,b) have shown that “tidal stirring” – or repeated tidal shocks suffered by dwarf satellite galaxies – can remove the kinematic signature from a low mass galaxy without significant alteration of its stellar distribution. While it is difficult to distinguish between these scenarios based on the data at hand,

the common feature of all of these scenarios is that non-rotating dwarf elliptical galaxies may have been significantly altered by their interaction with the cluster environment. Thus, it is possible that the galaxies which still retain their kinematic signature have been accreted relatively recently while the non-rotating dwarf elliptical galaxy sample may contain galaxies with a wide range of cluster accretion times, from the very recent to several Gyr in the past. Since it is likely that the age of the dominant stellar population is indicative of the time of accretion, observations of the stellar populations in these galaxies could provide insight into the accretion timescales.

In this paper, we analyze the past star formation activity in Virgo dwarf elliptical galaxies based on the combination of stellar population synthesis and spectral synthesis models. The imaging and spectroscopic observations are described in Section 2. We discuss the derived optical structural parameters of the dwarf elliptical galaxies in Section 3. In Section 4, we analyze the optical colors in the context of simple stellar populations. In Section 5, optical spectra are analyzed in the context of simple stellar population models to investigate typical timescales for chemical enrichment. The implications for the observed stellar population ages and enrichment histories are discussed in Section 6. The conclusions of the paper are summarized in Section 7.

2. Observations

Optical images were obtained of 16 dwarf elliptical galaxies with the VATT 1.8m and the WIYN 3.5m telescopes. Optical spectra were obtained with the Palomar 5m telescope. The kinematic results of the spectroscopic observations are presented in van Zee et al. (2004); here, we analyze the spectra in terms of stellar population models. The sample selection and observations are described in this section.

2.1. Sample Selection

As described in van Zee et al. (2004), the sample was selected to optimize the detection of rotational motion in dE galaxies. Sixteen dwarf elliptical galaxies were selected from the Virgo Cluster Catalog (VCC, Binggeli et al. 1985) based on their apparent luminosity ($m_B < 15.5$), morphological classification (dwarf elliptical or dS0), and apparent ellipticity ($\epsilon > 0.25$). The latter criterion was imposed to maximize the projected rotational velocity in the kinematic observations. In addition, the sample was restricted to those galaxies with measured recessional velocities that place them within the Virgo cluster, at an approximate distance of 16.1 Mpc (e.g., Kelson et al. 2000). Further details of the sample selection and distribution of the galaxies within the Virgo cluster are described in van Zee et al. (2004).

2.2. VATT 1.8m Observations

UBVRI images of 16 dwarf elliptical galaxies in the Virgo Cluster were obtained with the VATT 1.8m on 2003 March 29-31. The telescope was equipped with CCD26, a thinned Loral 3 2048 \times 2048 CCD with 15 μ m pixels. CCD26 has a read noise of 5.7 e⁻ and a gain of 1.9 e⁻ per ADU was used. On-chip binning of 2 \times 2 resulted in 0.375'' per pixel and a field of view of 6.4 \times 6.4 arcmin. The galaxies were centered in the field, but dithers of approximately 1 arcmin were taken between each exposure to assist with the flat fielding process.

Table 1 lists the basic parameters of the dE sample and summarizes the observations. Unless otherwise noted in Table 1, the VATT 1.8m observations consisted of 2 exposures of 540 sec, 420 sec, 300 sec, 240 sec, and 300 sec with the U, B, V, R, and I filters, respectively. Complete UBVRI images were obtained for 9 galaxies in the sample; BVRI images were obtained for an additional 4 galaxies and 3 galaxies were imaged in only B and R. The observations were structured so that the B and R images were obtained on the same night under similar observing conditions; similarly, the V and I images were taken sequentially. Thus, the (B-R) and (V-I) colors for these observations are quite secure, while (B-V) and (U-B) colors have additional error propagation terms since the colors are based on the calibrated magnitudes rather than calibration of the instrumental colors. The final combined images were sufficiently deep to permit accurate photometry of the outer regions of the galaxies. Typical surface brightness limits for the combined images are 25.8, 26.8, 26.0, 25.6, and 25.0 mag arcsec⁻², in U, B, V, R, and I, respectively.

All 3 nights were photometric. Calibration coefficients were derived from observations of standard stars from Landolt (1992) interspersed with the galaxy observations. Based on the derived photometric coefficients, the BVRI images have 2% accuracy while the U-band images are accurate to 3%.

2.3. WIYN 3.5m Observations

The same sample of galaxies was imaged with the WIYN³ 3.5m telescope on 2002 May 12-16. Poor weather hampered the usefulness of these observations, but the WIYN images provide confirmation for the structural parameters derived from the VATT 1.8m data. In particular, the WIYN images have slightly better seeing characteristics than the VATT 1.8m images.

The WIYN 3.5m telescope was equipped with the Mini-Mosaic camera, which consists of two SITe 4096 \times 2048 CCDs with 15 μ m pixels. The two CCDs are read-out by 4 amplifiers (2 per CCD), with typical read noises of 5.5 e⁻ and gains of 1.4 e⁻ per ADU. The pixel scale of Mini-Mo is 0.14'' per pixel, which results in a field of view of 9.6 \times 9.6 arcmin with a 7.1'' gap between the

³The WIYN Observatory is a joint facility of the University of Wisconsin-Madison, Indiana University, Yale University, and the National Optical Astronomy Observatories.

CCDs. In all cases, the telescope pointing was offset so that the dwarf elliptical galaxy fit on a single CCD.

The WIYN 3.5m observations consisted of 2 exposures of 600 sec, 600 sec, 300 sec, and 600 sec with the B, V, R, and I filters, respectively. R-band images were obtained for 13 of the 16 dEs in the sample; additional BVI images were obtained for 6 of the 13 galaxies. All 5 nights were non-photometric so the limiting surface brightness varied significantly from exposure to exposure. Typical image quality for the R-band WIYN images is 1-2".

2.4. Data Reduction of Optical Images

The optical images were reduced and analyzed with the IRAF⁴ package. The image reduction included bias subtraction and flat fielding. The VATT images were flat fielded to high accuracy using twilight flats. The WIYN 3.5m images were first flat fielded using dome flats taken during the afternoon; since these images had a residual flat field problem, a secondary flat field was generated from a combination of the object frames using standard tasks in the MSCRED package. Both the VATT and WIYN I-band images were fringe corrected based on a fringe frame generated by taking the median of all I-band galaxy observations obtained during the night.

For the WIYN images, data from the two CCDs must be projected onto a common coordinate system prior to further data processing. For each image, the WCS was updated using star lists from the USNO catalog and the IRAF tasks MSCZERO and MSCCMATCH. The multi-ccd images were then projected into single images using the MSCIMAGE task using a common coordinate system for all observations of the same galaxy.

For both the VATT and WIYN images, sky values were measured as the mode of galaxy-free regions of the images prior to combination of multiple exposures. The images were then scaled, aligned, and averaged together to make a final combined image. For the non-photometric observations (WIYN), the individual exposures were scaled to the image with the most counts; scale factors were determined based on the relative intensity of several stars in each frame. The VATT data were photometric and required no additional scaling before combination.

The VATT and WIYN images were processed independently in order to provide internal consistency checks for the derived structural parameters. Since the VATT images are photometric and higher quality than the WIYN images, the subsequent analysis will focus on results from the VATT observations.

⁴IRAF is distributed by the National Optical Astronomy Observatories.

2.5. Optical Spectroscopy

The optical spectroscopic observations are described in detail in van Zee et al. (2004). Briefly, optical spectra covering the wavelength ranges of 4800 – 5700 Å and 8250 – 8900 Å were obtained with the Double Spectrograph on the 5m Palomar⁵ telescope in 2001 and 2002. Here, we focus on the “blue” spectra, which were centered on the Mg Ib triplet and include a subset of the spectral regions appropriate for spectral synthesis using Lick/IDS indices. The observations were obtained on non-photometric, transparent nights. Flux calibration was obtained from observations of several spectrophotometric standards (Oke 1990) and observations of standard stars from the Lick/IDS system.

The long slit spectra were processed following standard practice [see van Zee et al. (2004) for complete data reduction details]. After bias subtraction, scattered light correction, flat fielding, wavelength rectification, and night sky line subtraction, the 2-dimensional (2-d) images were flux calibrated. One-dimensional (1-d) spectra were then extracted from the 2-d spectra to create spectra of the integrated light from the galaxy.

The 1-d spectra were Doppler corrected for the systemic velocity of the galaxies. Since the observed spectra have higher spectral resolution than the stellar spectra that define the Lick/IDS system, the 1-d spectra were then degraded from 1.6 Å resolution to 8.4 Å resolution. While the Lick indices are based on stellar spectra with variable resolution, the spectral region covered by these dE galaxy spectra correspond to a region of approximately constant spectral resolution in the Lick/IDS system (Worthey & Ottaviani 1997). Lick indices were then measured for the galaxies and the Lick standard stars. The observed spectra include the spectral regions appropriate for the following spectral indices: H β , Fe5015, Mgb, Fe5270, Fe5335, and Fe5406. In addition, similar to Geha et al. (2003), we define the average Fe index, $\langle Fe \rangle$, as the average of Fe5270 and Fe5335 indices.

The standard star observations were used to confirm that the indices measured here are consistent with previous measurements. However, since there were only a handful of comparison stars, and the stars observed comprise a restricted range of spectral types, it was not possible to determine a correction to the observed indices to place the measurements precisely on the Lick system. Nonetheless, for the few galaxies in common with the Geha et al. (2003) sample, the newly derived Lick indices are consistent with the previous measurements. Thus, while the derived indices may have some systematic errors, the amplitude of these errors should be minor. Furthermore, the *relative* measurements for the dE galaxies in this sample should be secure even if the absolute values may be less precise.

⁵Observations at the Palomar Observatory were made as part of a continuing cooperative agreement between Cornell University and the California Institute of Technology.

3. Structural Parameters

3.1. Surface photometry

The surface photometry for each galaxy was derived from ELLIPSE fits to the final combined images. Prior to ELLIPSE fitting, the foreground stars were masked and replaced by the interpolated background of neighboring pixels. The surface brightness profiles, position angle, and ellipticity are shown as a function of semi-major axis in Figure 1. Since the morphological parameters were similar for all filters, the apertures defined by the R-band fit were used for subsequent analysis of the surface brightness profiles and surface colors.

The morphological parameters are summarized in Table 2. Listed in Table 2 is the semi-major axis at which the B-band surface brightness drops to $25 \text{ mag arcsec}^{-2}$, R_{25} , and the average ellipticity and position angle from the isophotal fits of the R-band images for ellipses with semi-major axes between $5''$ and R_{25} . Apertures larger than $5''$ were used for these average values since several of the galaxies in this sample have bright nuclear regions. Also listed in Table 2 are the B-band apparent magnitudes at which the curves of growth level off and the observed optical colors as measured within the R_{25} aperture. As illustrated in Figure 1, the surface colors and aperture colors reach similar values near R_{25} so these values were chosen as the most representative galaxy color. Also tabulated in Table 2 are estimates of the foreground Galactic extinction as calculated from the dust maps of Schlegel et al. (1998).

The images were examined for residual disk or boxy isophotes by subtracting the model surface photometry from the image. Eleven of the 16 galaxies had residual structure that was readily apparent in the residual images; the presence of disk or boxy isophotes is tabulated in Table 2. Deviations from the best-fitting ellipse as measured by B_4 are shown in Figure 1.

As previously noted by Geha et al. (2003), there appears to be little correlation between the presence of disk or boxy residuals and the kinematic properties of the galaxies. As an indication of the kinematic properties of these galaxies, the rotation curve slope from van Zee et al. (2004) is listed in Table 2. Due to the limited spatial extent of the stellar kinematic observations, we list the rotation curve slope rather than a maximum velocity width; galaxies with rotation curve slopes greater than $20 \text{ km s}^{-1} \text{ kpc}^{-1}$ have significant rotation. Based on the kinematic observations, VCC 178, 437, 543, 965, 990, 1036, 1743, 1857, and 2019 form the subset of rotation dominated dEs in this sample.

Table 3 summarizes the derived photometric properties of the dwarf elliptical galaxies in this sample. The B-band absolute magnitude was calculated from the apparent magnitude assuming all galaxies are at the Virgo Cluster distance of 16.1 Mpc (Kelson et al. 2000) and correcting for Galactic extinction. Also listed are the effective radius and effective surface brightness in B-band. For all of the following except the exponential parameters, size parameters are quoted in geometric mean radii where $r = \sqrt{ab}$; for the exponential parameters, the semi-major axis is adopted as the radius. The effective radius tabulated in Table 3 is the half-light radius based on the apparent magnitude

listed in Table 2; the effective surface brightness is then defined as the average surface brightness within the R_{eff} elliptical aperture. We note that while these values are model independent, they can be sensitive to systematic errors introduced by shallow imaging observations since the half-light radii are defined based on the observed apparent magnitudes.

Several of the galaxies in this sample have surface photometry reported in the literature. Recent observations with partially overlapping samples include VCC 543, 917, 1036, 1261, and 1308 reported in Geha et al. (2003); VCC 965, 1036, 1122, and 1308 reported in Pierini (2002); VCC 1036 and 1261 reported in Barazza et al. (2003); and VCC 543 and 1743 reported in Durrell (1997). In general, there is reasonable agreement between the literature values and those reported here, particularly given the variety of filters and telescopes used by these studies. However, there are notable differences between the values reported here and the magnitudes and effective radii listed in Geha et al. (2003). With the exception of VCC 1261, it is likely that many of these differences can be attributed to differing image depths and to incomplete surface photometry as a result of the restricted field-of-view of HST imaging observations. For VCC 1261, the large discrepancy between the effective radius reported here and that reported in Geha et al. (2003) (more than a factor of 2) cannot be reconciled by mere observational differences; the present value agrees with the surface photometry of VCC 1261 reported in Barazza et al. (2003).

3.1.1. Exponential Fits

To enable comparison with galaxies of other morphological types, the outer isophotes ($r > 10''$) of the B-band surface brightness profiles were fit to an exponential model:

$$\mu(r) = \mu^0 + 1.086r/\alpha \quad (1)$$

where $\mu(r)$ is the observed surface brightness at semi-major axis r , μ^0 is the extrapolated central surface brightness, and α is the exponential scale length. The face-on central surface brightness, $\mu_B^{0,c}$, was calculated by applying a Galactic extinction correction and a line-of-sight correction of $-2.5 \log(\cos i)$, where i is the inclination derived from the observed axial ratios and a thin disk approximation. While an exponential distribution does not necessarily imply a disk-like stellar distribution, the simplicity of this functional form permits a robust analysis of the light distribution of the outer regions of a galaxy, regardless of the actual shape of the galaxy (disk or spheroid). The exponential fits enable a direct comparison between the structural parameters of dE and dI galaxies (Figure 2). The top panel of Figure 2 shows the scale length as a function of absolute magnitude while the bottom panel shows the face-on central surface brightness as a function of absolute magnitude. For comparison, the structural parameters for dwarf irregular galaxies from van Zee (2000) are also shown. Despite the fact that this comparison sample may not be ideal, since the dIs were selected to be isolated galaxies and the dEs are cluster members, these figures confirm that the structural parameters of dIs and dEs are quite similar (as first discussed in Lin & Faber 1983). In particular, both the dI and dE samples contain low surface brightness galaxies

with typical central surface brightnesses between 22 to 24 mag arcsec⁻² and scale lengths of only a few kpc.

3.1.2. Sérsic Fits

While the parameters for an exponential fit are sufficient to represent the stellar distribution in the outer galaxy, a more generalized surface brightness profile, such as the Sérsic function (Sérsic 1968), can provide additional insight into the stellar distribution. The surface brightness profiles were fit to a Sérsic function of the form: $I = I_0 e^{-(r/r_0)^n}$. In magnitude space, this corresponds to

$$\mu = \mu_s + 1.0857(r/r_s)^n \quad (2)$$

where μ_s is the central surface brightness, r_s is a size parameter, and n is a shape parameter. In this form, $n=0.25$ corresponds to an $R^{1/4}$ law distribution, while $n=1$ corresponds to an exponential (disk) distribution. The surface brightness profiles were fit for geometric mean radii between 1'' and the radius at which the R-band surface brightness reached 25 mag arcsec⁻². Since the derived parameters were similar regardless of filter choice, only the R-band fits are listed in Table 3 and shown in Figure 1. In general, the surface brightness profiles were well fit by the Sérsic function, with shape parameters, n , between 0.5 and 1. However, the Sérsic parameterization proved to be quite sensitive to choice of fitting radii. Thus, while errors are listed in Table 3, equally valid solutions can be found with parameterizations that are outside of the range apparently permitted by these formal errors.

Several of the galaxies in this sample have Sérsic parameters listed in the literature. The present results agree with the literature values for VCC 1036 and 1261 (Barazza et al. 2003), VCC 1308 (Geha et al. 2003), and VCC 1743 (Durrell 1997). However, when overlayed with the observed surface brightness profile, the Sérsic parameters for VCC 543, 917, and 1035 from Geha et al. (2003) yielded good fits only to the inner regions of these galaxies (as mentioned above, their values for VCC 1261 do not match the surface brightness profiles obtained here). Similarly, the parameters listed in Durrell (1997) for VCC 543 are only applicable to the inner profile. The disagreement between the present study and the literature is not surprising since Sérsic fits are sensitive to the choice of fitting radii, and the previous analysis often restricted the fits to the inner 20-30''.

The results of Sérsic fits for dwarf elliptical galaxies in the Virgo Cluster are shown in Figure 3. Figure 3 includes all dE galaxies fainter than M_B of -17.5 with published kinematic data (e.g., the sample includes galaxies compiled from Pedraz et al. 2002; Geha et al. 2003). Structural parameters for many of the galaxies in Pedraz et al. (2002) and Geha et al. (2003) were compiled from Barazza et al. (2003). For those galaxies in Geha et al. (2003) without published B-band effective surface brightnesses, the published V-band effective surface brightness was converted to an approximate B-band value by assuming that the typical (B-V) color of a Virgo dE is 0.77 (see Section 4.2). While Figure 3 indicates that there is a general trend of larger shape parameters (n) for fainter dwarf ellipticals, and for brighter central surface brightnesses for brighter galaxies, the rotating and

non-rotating dwarf elliptical galaxies cannot be distinguished in any of these figures. In fact, the kinematic samples are well mixed in terms of shape, surface brightness, and size.

In summary, there appear to be no strong morphological differences between rotating and non-rotating dwarf elliptical galaxies in the Virgo cluster. Underlying disk and boxy isophotes are seen in both kinematic samples (see also Geha et al. 2003). The structural parameters are similar as well. In the next section, we investigate whether there are stellar population differences between the rotating and non-rotating dwarf elliptical galaxies.

4. Optical Colors and Color Gradients of Dwarf Elliptical Galaxies

4.1. Optical Color Gradients

As illustrated in Figure 1, many of the dwarf elliptical galaxies in this sample have a slight color gradient. However, this trend does not appear to be correlated with the presence of a nucleated region; several of the nucleated dEs have no color gradients while several of the non-nucleated dEs do have a color gradient. Color gradients are commonly seen in dEs, usually in the sense that the outer regions are redder than the inner regions (Vader et al. 1988; Jerjen, Binggeli, & Freeman 2000; Barazza et al. 2003). In this sample, VCC 965, 1743, 1857, and 2019 have color gradients in this expected direction. However, approximately one half of the current sample have color gradients in the opposite sense; the inner regions are redder than the outer regions of VCC 178, 543, 917, 990, 1036, 1122, 2050.

A color gradient implies differing star formation histories, or differing metal content, in the inner and outer regions of the galaxy. It is likely that both of these effects are relevant to the interpretation of observed colors and stellar populations of Virgo dEs. For example, a galaxy may develop a color gradient if the outer gas is preferentially stripped off as it falls into the Virgo cluster. In this scenario, the inner region of the galaxy may continue to have active star formation while the outer regions are reduced to an aging stellar population (redder colors). Such a scenario easily explains the observed color gradients in most dwarf elliptical galaxies (redder in the outskirts). Alternatively, a color gradient in the opposite sense can be created if the inner region retains a larger fraction of its enriched material; if there is a metallicity gradient, the more metal-rich stars (inner regions) will be redder than the metal-poor stars (outskirts). The relative importance of both of these effects will depend on the galaxy’s detailed star formation history and the interface of the galaxy with the intracluster medium.

As shown in Figure 4, the presence of a color gradient does not correlate with the kinematic properties of the dEs. Galaxies with a blue core (VCC 965 and 2019) or red core (VCC 543, 917, 990, 1036, and 2050) are equally likely to be rotation dominated as galaxies with no strong color gradient. Also shown in Figure 4 is the luminosity-line width correlation for spiral galaxies (Tully & Pierce 2000) and for field dwarf irregular galaxies compiled in van Zee (2001). As discussed

in van Zee et al. (2004), the observed dE rotation velocities are lower limits due to observational constraints; reasonable extrapolation of the observed rotation curves result in linewidths comparable to galaxies that are 1-2 magnitudes brighter than the current dE population. This fading estimate is in reasonable agreement with that expected if dEs are evolved dIs (e.g., Bothun et al. 1986). Nonetheless, it is quite remarkable that the observed (un-extrapolated) rotation velocities show excellent agreement with the bright galaxy Tully-Fisher relation.

4.2. Optical Colors

The presence of a color gradient complicates the definition of a global galaxy color. To avoid systematic trends due to nuclear contamination of the colors, the colors tabulated in Table 2 are measured within the B-band 25 mag arcsec⁻² isophotal aperture; this aperture color was selected to be representative of the true color of the galaxies since the aperture and surface colors are quite similar at this radius (see Figure 1). Table 3 lists the observed optical colors corrected for Galactic extinction. The optical colors are remarkably similar for all of the dEs in this sample. The median colors are 0.24 ± 0.03 in (U–B), 0.77 ± 0.02 in (B–V), 1.26 ± 0.05 in (B–R), 0.48 ± 0.01 in (V–R), and 1.02 ± 0.03 in (V–I). Observations of low luminosity elliptical galaxies yield similar colors for galaxies in the same absolute magnitude range (Prugniel et al. 1993).

The optical colors are shown in Figure 5; as expected, the dwarf elliptical galaxies are red systems in all color combinations. For comparison, the evolutionary tracks for 3 possible star formation histories are shown in Figure 5. The evolutionary tracks are obtained from the simple stellar population models of Bruzual & Charlot (2003) assuming a mean metallicity of 1/5 solar; the low metallicity stellar population models were selected for this figure because low luminosity galaxies are usually low metallicity systems (e.g., Skillman, Kennicutt, & Hodge 1989; Richer & McCall 1995). The Bruzual & Charlot (2003) galaxy evolution code is an improved version of the composite stellar population models originally described in Bruzual & Charlot (1993). As in Bruzual & Charlot (1993), the mono-metallicity composite stellar populations are built through the synthesis of stellar evolutionary tracks (e.g., Lejeune et al. 1997). The version of the galaxy evolution code run here includes options for sub- and super-solar metallicity stellar populations, in addition to allowing the user to vary the star formation history and the initial mass function. For simplicity, a Salpeter (1955) IMF was adopted for all of the models considered here; a top- or bottom-heavy IMF will result in minor variations in the evolutionary tracks, but relative conclusions should be robust with regard to the choice of IMF.

The three fiducial star formation histories shown in Figure 5 include (1) a simple burst of star formation that lasts 10 Myr, (2) an extended burst of star formation with an e-folding time of 1 Gyr ($\tau = 1$), and (3) a constant star formation rate model. As expected, the constant star formation rate model can be ruled out for the Virgo dEs since these galaxies have no current star formation activity; this model is appropriate for dwarf irregular galaxies which have quasi-continuous star formation activity (van Zee 2001). The observed colors are consistent with both fiducial star burst

models (short and extended starbursts). In both cases, the observed colors are indicative of an older stellar population with an age of approximately 6 Gyr. While there is some ambiguity in this age estimate due both to the well known age-metallicity degeneracy and to possible different star formation histories, it is clear that the observed colors are indicative of a stellar population which has had little-to-no star formation activity within the last few Gyr. Thus, while the observed broad band colors do not permit a detailed analysis of the past star formation activity in these galaxies, they do indicate that none of the galaxies in this sample are *recently* stripped dwarf irregular galaxies.

Further, the small range of observed colors for the galaxies in this sample indicates that the dominant stellar population is quite similar for both the rotating and non-rotating dwarf elliptical galaxies. As illustrated in Figure 6, much of the scatter in the observed colors can be attributed to the well known color-magnitude relation for dwarf elliptical galaxies (e.g., Caldwell 1983). In general, the more luminous galaxies in this sample are slightly redder, as would be expected if the more luminous galaxies in the sample are also more metal-rich (e.g., Skillman, Kennicutt, & Hodge 1989). The two significant outliers to this relation are VCC 1857 and VCC 1261, both of which are bluer than one might expect for their absolute magnitude. Interestingly, neither of these galaxies have a significant color gradient, so their anomalous colors cannot be explained by nuclear contamination. We note also that the present results for VCC 1261 are consistent with the B-R color reported in Barazza et al. (2003) for this galaxy. It is suggestive that VCC 1857 is not only bluer than expected, but also has slightly different structural parameters than the other Virgo dEs; this galaxy is the best candidate in this sample for a recently stripped dI. Nonetheless, its optical colors are still consistent with an older stellar population, indicating that the last star formation activity occurred several Gyr ago. Unfortunately, the kinematic observations of VCC 1857 were inconclusive; while the derived rotation curve indicates that VCC 1857 may have a significant rotational component, the rotation curve was poorly constrained because of the galaxy’s low surface brightness nature. In contrast, the other anomalous galaxy, VCC 1261, is the one galaxy in the sample with clear absence of a rotational component along its major axis.

Using these two outliers as indicative examples, the relative colors of the Virgo dEs do not appear to be related to their kinematic signatures. Rather, the small range of observed colors for the galaxies in this sample indicates that the ages of the dominant stellar population are approximately the same for both rotating and non-rotating dwarf elliptical galaxies. We note, however, that broad band colors do not permit a detailed analysis of the past star formation activity in these galaxies since the observed colors are consistent with both a short burst and with a more extended star formation history. We explore additional constraints on the past star formation activity by examining the chemical signatures of the dominant stellar population in the next section.

5. Age and Metallicity: Spectroscopic Evidence

The results of the spectral analysis are shown in Figure 7. The expected Lick indices for three possible $[\alpha/\text{Fe}]$ ratios are shown based on the models of Thomas et al. (2003b). Unlike giant elliptical galaxies, the majority of dwarf elliptical galaxies in Virgo appear to have solar or sub-solar $[\alpha/\text{Fe}]$ ratios. Similar results are found by Geha et al. (2003) and Thomas et al. (2003a) for their samples of Virgo dwarf elliptical galaxies; in addition, similar $[\alpha/\text{Fe}]$ ratios are seen in stellar abundances of nearby dwarf spheroidals (e.g., Shetrone et al. 2001, 2003). Since Type II supernova produce the majority of α -rich elements, the observed $[\alpha/\text{Fe}]$ ratios trace the timescale of star formation activity in each galaxy (Gilmore & Wyse 1991). In particular, super-solar $[\alpha/\text{Fe}]$ indicates rapid enrichment from Type II supernova and thus implies that the galaxy has undergone a short burst of star formation activity; most giant elliptical galaxies have super-solar $[\alpha/\text{Fe}]$ (e.g., Trager et al. 2000). In contrast, the solar and sub-solar abundance ratios for dEs indicate slow chemical enrichment, or a more quiescent star formation history. Thus, the dominant stellar populations in Virgo dEs may not be post-burst populations. Rather, previous star formation activity appears to have occurred on more extended timescales in the low mass galaxies; these and similar results (e.g., Gallagher & Wyse 1994; Mateo 1998) rule out various theoretical models for dE formation, including the possibility that dEs and dSphs form all stars prior to reionization (e.g., Barkana & Loeb 1999). The observed $[\alpha/\text{Fe}]$ ratios are consistent with the idea that Virgo dEs are formed through the stripping of dIs; if star formation activity ceases when the ISM is removed from the low mass system, the galaxy will evolve into a quiescent, red galaxy with structural and kinematic parameters similar to the progenitor dI, and with a chemical enrichment history representative of a more continuous star formation history.

Comparison of the $\text{H}\beta$ and Mgb indices provides an indication of the age of the dominant stellar population in the dEs (Figure 8). Also shown in Figure 8 are the stellar population models of Thomas et al. (2003b) for solar $[\alpha/\text{Fe}]$. As expected from the optical colors (Section 4), the stellar populations are both metal-poor and evolved. Based on these observations and stellar population models, Virgo dEs have typical ages of 5-7 Gyr and metal abundances between 1/20 and 1/3 of solar. Similar results for Virgo dEs were also obtained by Geha et al. (2003). The derived age and metallicity estimates for these galaxies are also in remarkably good agreement with those obtained from the broad band optical images. As found with the optical colors, there is no clear separation of the kinematic samples in either age or metallicity of the dominant stellar population. Thus, both stellar population models and spectral synthesis indicate that Virgo dEs contain evolved low metallicity stellar populations with typical ages of a several Gyr and solar or sub-solar $[\alpha/\text{Fe}]$.

6. Discussion

The derived structural parameters and metal enrichment histories indicate that the Virgo dEs are similar in nature to field dwarf irregular galaxies with the exception of the age of the dominant

stellar population. Thus, the current observations are consistent with the idea that some cluster dEs are the remnants of dIs which have been stripped of their ISM. Taken at face value, the derived mean stellar population ages indicate that the last major star formation episode in the Virgo dEs occurred 5-7 Gyr ago, or at $z > 0.5$. However, due to the inherent ambiguities in stellar population models, it is difficult to determine exactly how long it has been since star formation occurred in these galaxies. For example, the observed colors are not only consistent with the two burst models discussed above (extended starburst and short burst), but also with a galaxy which has had a constant star formation rate which is abruptly truncated 3 Gyr ago ($z \sim 0.3$). Unfortunately, the Virgo dwarfs are too distant to produce detailed star formation histories as is possible within the Local Group (e.g., Skillman et al. 2003). Nonetheless, all of these models indicate that the Virgo dEs have not had substantial star formation activity within the last few Gyr.

Furthermore, the observed $[\alpha/\text{Fe}]$ ratios are solar or sub-solar, indicating that the stellar mass of the cluster dEs has been built gradually, rather than through a major burst of star formation. Thus, not only do low mass cluster galaxies have different structural properties than their giant cousins, their stellar populations and star formation histories appear to be substantially different. While both giant and dwarf elliptical galaxies appear to have strong environmental dependences on their formation and evolution, it is likely that low mass cluster galaxies follow different evolutionary paths than their giant counterparts. For example, interactions with the cluster potential and the ICM may be the key to formation of dEs, while galaxy-galaxy interactions may play a major role in the evolution of giant ellipticals.

6.1. Are the Majority of Virgo dEs Produced by the Infall and Stripping of dIs?

Since the early recognition of similar structural parameters between dE and dI galaxies (e.g., Lin & Faber 1983; Kormendy 1985), it has often been suggested that dEs could simply be dIs stripped of their gas and left to fade. The extensive study of the Virgo cluster resulting in the VCC (c.f., Binggeli et al. 1985; Sandage, Binggeli, & Tammann 1985; Binggeli et al. 1987) confirmed the strong overlap between these two populations, but led Binggeli (1985) to conclude that the dEs are not formed from dIs due to the apparent lack of a bright progenitor dI population and to the presence of bright nuclei in a large fraction of dEs. While Binggeli (1985) was careful to note that his arguments applied only to the brightest dEs, he argued that if one could not explain the entire dE population with stripping then it did not make sense to invoke this process since it is inelegant to explain the well defined sequence in L , α , μ space with more than one process.

In van Zee et al. (2004), we proposed that Virgo dEs are formed through multiple processes. First, it is likely that the most massive galaxies near the core of the cluster formed with a coterie of satellite galaxies, which soon became dE galaxies. However, we also know that the Virgo cluster is still forming today, and that field galaxies and groups of galaxies are falling into the cluster (Tully & Shaya 1984; Binggeli et al. 1987). If the groups of galaxies that later fell into the Virgo cluster were similar to our Local Group, then they likely consisted of roughly equal numbers of

dE and dI galaxies before entering the cluster environment. In addition, the infalling dI galaxies are likely to be affected by the cluster environment and may lose their ISM through ram pressure stripping or through interactions with other galaxies. It therefore seems unavoidable that there are at least three different origins for the Virgo dEs (*in situ* formation near massive elliptical galaxies, infalling dEs that were once part of Local Group analogs, and converted infalling dIs). Thus, the narrow locus formed by dEs in structural parameter space may better be interpreted as the result of an inevitable structural form as opposed to a uniform process of creation. In other words, the uniformity of dE/dI properties may be due more to the uniformity of their dark matter halos (Navarro, Frenk, & White 1997), rather than a single formation mechanism.

Additional arguments have been made against the stripping of infalling dIs to form the Virgo dE population. Gallagher & Hunter (1989) reason that the scarcity of dwarf galaxies with blue colors and low HI content argues against extensive stripping of dI systems in the last \sim Gyr. However, recent observations have identified several likely candidates as recently stripped dIs. The best case for stripping of a dwarf galaxy in process is that of the HI cloud between NGC 4472 and UGC 7636 discovered by Sancisi, Thonnard, & Ekers (1987). Subsequent observations of this system have shown that the morphologies of the optical galaxy and the HI cloud, although separated by 15 kpc, are “remarkably similar” (McNamara et al. 1994) and that the ISM abundance of the cloud agrees with that expected for the luminosity of UGC 7636 (Lee, Richer, & McCall 2000) - essentially clinching the proposal that this is a recent stripping event. Lee, Kim, & Geisler (1997) found blue star clusters with ages up to 10^8 yrs associated with both the optical galaxy and the HI cloud and this provides a minimum time since the stripping event. In addition to UGC 7636, IC 3475 has been identified as a recently stripped irregular galaxy (Vigroux et al. 1986), IC 3365 appears to be a dI caught in the act of being stripped (Skillman et al. 1987), and VCC 882 is a nucleated dE that from a long trail of dust appears to have recently been stripped of its ISM (Elmegreen et al. 2000).

Anecdotal evidence allows us to be sure that the process of ram pressure stripping is viable, but a statistical approach is required to address the point made by Gallagher & Hunter (1989). From a large sample of HI observations of Virgo dIs, Hoffman et al. (1985) concluded that the HI depletion of dIs is only moderate. However, this was based on comparing M_{H}/L ratios of dIs to those of spirals. The means of 0.2 for the bright Virgo dIs and 0.5 for the faint Virgo dIs are both significantly smaller than the typical M_{H}/L of 1 for field dIs (e.g., Fisher & Tully 1975; van Zee et al. 1995; Skillman 1996). From this, one can conclude that a significant fraction of Virgo dIs are showing the effects of the cluster environment. Lee, McCall, & Richer (2003) have revisited this question, and a comparison of Virgo dIs with field dIs show the majority of Virgo dIs in their sample have HI deficiencies. Finally, from our color and spectroscopic dating of Virgo dEs, it is clear that the majority have been dEs for several Gyr. If most of the conversions happened long ago, a low transformation rate today might only imply that the process is slowing down, rather than excluding it altogether. In fact, the argument is based on the assumption of a constant rate of creation of dEs over the Hubble time. Given the stochastic nature of infall, a variable rate of infall would also be consistent with a low rate of dE creation in the present epoch and a large population

of dEs formed from stripped dIs.

Arguments against conversion from dIs to dEs by ram pressure stripping have also been made on theoretical grounds. Ferguson & Binggeli (1994) revisit this question and offer a rough calculation of the time scale for ram pressure stripping and note that it is unreasonably long for distances greater than 300 kpc from M87 (which excludes only the very core of the Virgo cluster). They conclude that “stripping was probably not the dominant gas-removal mechanism” in the Virgo cluster. However, they note that a more realistic treatment of the ISM in a dI might yield significantly shorter gas removal times. The empirical counter example to this theoretical calculation comes in the form of HI observations of the spiral galaxy NGC 4522 (Kenney, van Gorkom, & Vollmer 2004). They show this $0.5 L^*$ galaxy to be undergoing significant stripping at a projected distance of ~ 800 kpc from M 87. The stripping of the HI is complete to significantly higher mass surface densities than seen in most dwarf galaxies, and thus any gas rich dwarf in this environment is likely to be stripped.

Binggeli’s (1985) argument concerning the lack of a progenitor population for nucleated dEs remains as a possible constraint on the number of Virgo dEs which are created as a result of stripping of an infalling dI. Unfortunately, without a consensus view on the formation of the nuclei of nucleated dEs (see, e.g., Oh & Lin 2000; Binggeli, Barazza, & Jerjen 2000), it is difficult to judge the strength of this constraint. The fact that the nucleated dEs are more strongly clustered than the non-nucleated dEs (e.g., Binggeli et al. 1987) may be an indication that they are part of an *in situ* population of galaxies formed as satellites of the original cluster galaxies. Based on specific globular cluster frequencies, Miller et al. (1998) propose that the non-nucleated dEs are the more likely dEs to form as a result of stripping. However, in this regard, note that 3 of the 5 galaxies in the van Zee et al. (2004) sample with strong rotational support ($v/\sigma > 1$) are nucleated dEs. Alternatively, it is possible that nucleated dEs could be formed from dIs with large central starbursts (Davies & Phillipps 1988). Further study of their stellar populations and structure are needed to understand fully the origin of the nuclei and thus to determine if stripped dIs can evolve into nucleated dwarf ellipticals.

Finally, a possible concern for dI to dE evolution through ram pressure stripping is a possible disparity in baryon-to-dark matter ratios in these low mass galaxies. While the characteristics of the dark matter halos of the Local Group dSph galaxies are currently a matter of debate (cf., Kleyna et al. 2002; Piatek et al. 2002; Stoehr et al. 2002; Palma et al. 2003), it appears that dSph may have lower dark matter-to-luminosity ratios than similar luminosity dwarf irregular galaxies (e.g., Mateo 1998). However, such results should be viewed with some caution since dark matter halos are measured in different ways for rotating and non-rotating systems (Mateo 1998). Thus, at this time, possible discrepancies in the masses of dark matter halos and baryon-to-dark matter ratios of non-rotating Virgo dEs are not sufficiently robust to exclude ram pressure stripping as a viable evolutionary pathway from dI to dE. Further, as shown in Figure 4, the rotating Virgo dEs have maximum rotation velocities comparable to similar luminosity dIs, suggesting that at least this subset of dE galaxies may have similar baryon-to-dark matter ratios as field dIs.

In summary, after reviewing the historical comparisons of the dE and dI populations in Virgo which have been used to rule out the creation of the Virgo dEs by infalling dIs, we find no observational evidence which rules out the creation of a majority of the Virgo dEs by the stripping of gas from dIs. We note, however, that if ram pressure stripping is a common mechanism for transforming dIs to dEs, there remains a fundamental difficulty of identifying the population of recently stripped dIs. In all likelihood, the recently stripped dIs are not (yet) classified as dEs (UGC 7636 is dI). In fact, any young stellar population must have already faded by the time a galaxy is classified as a dE since the primary morphological criterion is that dEs have smooth and regular isophotes. Thus, it should not be surprising that all the dEs in this sample have similar optical colors. By the time a galaxy is classified as a dE, its stellar population has aged sufficiently (~ 2 Gyr) that the observed colors are red and it is no longer possible to determine a precise time since the last star formation episode. In analogy with the Local Group dSph, however, it is likely that the detailed star formation histories of the Virgo dEs (as revealed by color magnitude diagrams) will differ substantially even though the integrated colors are similar.

6.2. Are the Rotating dEs and Non-Rotating dEs Formed Differently?

The optical images and spectroscopy presented here indicate that there are no obvious differences between the stellar populations of rotating and non-rotating dwarf elliptical galaxies. In van Zee et al. (2004), we proposed the possibility that non-rotating dEs may have entered the cluster environment as dEs, while rotating dEs may have been converted from dIs while entering the cluster environment. If this scenario is correct, then one would expect, on average, that the non-rotating dEs would have older stellar populations. Unfortunately, the age resolution afforded by the present observations and the sample size are insufficient to provide a clear test. There is the additional complication that a rotationally supported dE which is a result of a ram pressure stripping event may follow a trajectory in which a close encounter significantly alters its kinematics (e.g., Mayer et al. 2001b). Thus, even if the rotating and non-rotating dEs are entering the cluster environment in similar distributions, the distributions of the observed rotating and non-rotating dEs could be significantly different.

The best way to sort out this question observationally may be to study the population of recently stripped galaxies and those galaxies being actively stripped today. An unbiased HI survey of the Virgo cluster environment may reveal a large number of HI clouds similar to the one associated with UGC 7636. If so, then the distribution (in both real space and velocity space) of these objects and their association with rotating or non-rotating galaxies will offer significant constraints on all scenarios accounting for the dE population in Virgo. The new seven feed L-Band array (ALFA) at Arecibo Observatory is well suited to such a blind neutral hydrogen survey. With a relatively small beam (3 arcmin), ALFA observations of the Virgo cluster will have sufficient spatial resolution and sensitivity to identify recently stripped HI clouds and gas-poor dwarf irregular galaxies within this high density region; such observations will improve significantly our understanding of the population

and location of recently stripped dIs and their connection to the dwarf elliptical population.

6.3. Are Intermediate- z Faint Blue Galaxies the Progenitors of Dwarf Ellipticals?

The abundant dE population in the local universe implies the existence of a large population of star forming dwarf galaxies at intermediate redshifts, corresponding to progenitors of the local dE population. The detectability and the nature of this population depend entirely on the evolutionary histories of dEs. If dEs build stellar mass rapidly, they could appear as luminous objects ($> L^*$) during their formation and then fade by > 3 magnitudes to the present epoch. Such “starburst” scenarios are favored to explain the rapidly evolving population of faint blue galaxies at intermediate redshift (e.g. Babul & Rees 1992). However, the observed $[\alpha/\text{Fe}]$ indicates that dEs build their stellar mass more slowly. If most dEs form from dIs, with their roughly constant star formation histories punctuated by, at most, moderate bursts of star formation, the forming dEs may be only 1-2 magnitudes brighter than those at the present epoch. Thus, with expected magnitudes $M_B \geq -18$ ($m_R > 24$ at $z = 0.5$), the population of dE progenitors will be rare in most extragalactic surveys.

We caution, however, that integrated colors and elemental abundance ratios provide only modest constraints on the detailed star formation history of a galaxy since a modest star burst, or period of quiescence, can be masked by subsequent star formation episodes. Thus, while the present observations are suggestive that the dI to dE transition does not require a starburst episode, observations of the resolved stellar populations will be necessary to determine the detailed star formation history of dwarf elliptical galaxies. Such observations are beyond the capabilities of current optical telescopes, but the next generation of ground based telescopes may make this a realistic goal even at the distance of the Virgo cluster. Such observations are crucial for our understanding and interpretation of galaxy counts at moderate to high redshift.

7. Conclusions

We present optical images and spectral synthesis of 16 dwarf elliptical galaxies in the Virgo cluster. The major results of these observations are as follows:

(1) There appear to be no major morphological differences between rotating and non-rotating dwarf elliptical galaxies. Underlying boxy and disk isophotes are seen in both kinematic samples. As first discussed by Lin & Faber (1983) and Kormendy (1985), the cluster dEs have similar structural parameters as field dIs.

(2) The global optical colors are red, with median values for the sample of 0.24 ± 0.03 in (U–B), 0.77 ± 0.02 in (B–V), 1.26 ± 0.05 in (B–R), 0.48 ± 0.01 in (V–R), and 1.02 ± 0.03 in (V–I).

(3) Stellar population models and spectral synthesis indicate that the dominant stellar populations have ages of approximately 5-7 Gyr. Based on Lick indices and simple stellar population

models, the derived $[\alpha/\text{Fe}]$ ratios are sub-solar to solar, indicating a more gradual chemical enrichment history for dEs as compared to giant elliptical galaxies in the Virgo Cluster.

(4) We argue that it is likely that several different physical mechanisms played a significant role in the production of the Virgo cluster dE galaxies including *in situ* formation, infall of dEs that were once part of Local Group analogs, and the conversion of infalling dIs. The present observations support the hypothesis that a large fraction of the Virgo cluster dEs are formed by ram pressure stripping of gas from infalling dIs.

This research has made use of the NASA/IPAC Extragalactic Database (NED) which is operated by the Jet Propulsion Laboratory, California Institute of Technology, under contract with the National Aeronautics and Space Administration. We thank the VATT time allocation committee for awarding TBS time to complete this project. LvZ acknowledges partial support by Indiana University. Support for EJB was provided by NASA through Hubble Fellowship grant #HST-HF-01135.01 awarded by the Space Telescope Science Institute, which is operated by the Association of Universities for Research in Astronomy, Inc., for NASA, under contract NAS 5-26555. EDS is grateful for partial support from a NASA LTSARP grant No. NAG5-9221 and the University of Minnesota.

REFERENCES

- Babul, A., & Rees, M. J. 1992, MNRAS, 255, 346
- Barazza, F. D., Binggeli, B., & Jerjen, H. 2003, A&A, 407, 121
- Barkana, R., & Loeb, A. 1999, ApJ, 523, 54
- Binggeli, B. 1985, in Star-Forming Dwarf Galaxies and Related Objects. Kunth, D., Thuan, T. X., Tran Thanh Van, J. (eds) Éditions Frontières, Gif Sur Yvette, p.53
- Binggeli, B., Barazza, F., & Jerjen, H. 2000, A&A, 359, 447
- Binggeli, B., & Cameron, L. M. 1991, A&A, 252, 27
- Binggeli, B., Sandage, A., & Tammann, G. A. 1985, AJ, 90, 1681
- Binggeli, B., Tammann, G. A., & Sandage, A. 1987, AJ, 94, 251
- Binggeli, B., Tarenghi, M., & Sandage, A. 1990, A&A, 228, 42
- Bothun, G. D., Mould, J. R., Caldwell, N., & MacGillivray, H. T. 1986, AJ, 92, 1007
- Bruzual A., G., & Charlot, S. 1993, ApJ, 405, 538
- Bruzual, G., & Charlot, S. 2003, MNRAS, 344, 1000

- Caldwell, N. 1983, *AJ*, 88, 804
- Caldwell, N., & Bothun, G. D. 1987, *AJ*, 94, 1126
- Davies, J. I., & Phillipps, S. 1988, *MNRAS*, 233, 553
- Dekel, A., & Silk, J. 1986, *ApJ*, 303, 39
- Dressler, A. 1980, *ApJ*, 236, 351
- Durrell, P. R. 1997, *AJ*, 113, 531
- Elmegreen, D. M., Elmegreen, B. G., Chromey, F. R., & Fine, M. S. 2000, *AJ*, 120, 733
- Ferguson, H. C., & Binggeli, B. 1994, *A&A Rev.*, 6, 67
- Fisher, J. R. & Tully, R. B. 1975, *A&A*, 44, 151
- Gallagher, J. S., & Hunter, D. A. 1989, *AJ*, 98, 806
- Gallagher, J. S., III. & Wyse, R. F. G. 1994, *PASP*, 106, 1225
- Geha, M., Guhathakurta, P., & van der Marel, R. P. 2003, *AJ*, 126, 1794
- Gilmore, G., & Wyse, R. F. G. 1991, *ApJ*, 367, L55
- Hoffman, G. L., Helou, G., Salpeter, E. E., & Sandage, A. 1985, *ApJ*, 289, L15
- Ichikawa, S.-I., Wakamatsu, K.-I., & Okamura, S. 1986, *ApJS*, 60, 475
- Impey, C., Bothun, G., & Malin, D. 1988, *ApJ*, 330, 634
- Jerjen, H., Binggeli, B., & Barazza, F.D. 2004, *AJ*, 127, 771
- Jerjen, H., Binggeli, B., & Freeman, K. C. 2000, *AJ*, 119, 593
- Kelson, D. D. et al. 2000, *ApJ*, 529, 768
- Kenney, J. D. P., van Gorkom, J. H., & Vollmer, B. 2004, *AJ*, 127, 3361
- Kleyna, J., Wilkinson, M. I., Evans, N. W., Gilmore, G., & Frayn, C. 2002, *MNRAS*, 330, 792
- Kormendy, J. 1985, *ApJ*, 295, 73
- Landolt, A. U. 1992, *AJ*, 104, 340
- Lee, M. G., Kim, E., & Geisler, D. 1997, *AJ*, 114, 1824
- Lee, H., McCall, M. L., & Richer, M. G. 2003, *AJ*, 125, 2975
- Lee, H., Richer, M. G., & McCall, M. L. 2000, *ApJ*, 530, L17

- Lejeune, Th., Cuisinier, F., & Buser, R. 1997, *A&AS*, 125, 229
- Lin, D. N. C., & Faber, S. M. 1983, *ApJ*, 266, L21
- Mateo, M. L. 1998, *ARA&A*, 36, 435
- Mayer, L., Governato, F., Colpi, M., Moore, B., Quinn, T., Wadsley, J., Stadel, J., & Lake, G. 2001a, *ApJ*, 547, L123
- Mayer, L., Governato, F., Colpi, M., Moore, B., Quinn, T., Wadsley, J., Stadel, J., & Lake, G. 2001b, *ApJ*, 559, 754
- McNamara, B. R., Sancisi, R., Henning, P. A., & Junor, W. 1994, *AJ*, 108, 844
- Miller, B. W., Lotz, J. M., Ferguson, H. C., Stiavelli, M., & Whitmore, B. C. 1998, *ApJ*, 508, L133
- Navarro, J. F., Frenk, C. S., & White, S. D. M. 1997, *ApJ*, 490, 493
- Neilsen, E. H. Jr., & Tsvetanov, Z. I. 2000, *ApJ*, 536, 155
- Oh, K. S. & Lin, D. N. C. 2000, *ApJ*, 543, 620
- Oke, J. B. 1990, *AJ*, 99, 1621
- Palma, C., Majewski, S. R., Siegel, M. H., Patterson, R. J., Ostheimer, J. C., & Link, R. 2003, *AJ*, 125, 1352
- Pedraz, S., Gorgas, J., Cardiel, N., Sánchez-Blázquez, P., & Guzmán, R. 2002, *MNRAS*, 332, L59
- Piatek, S., Pryor, C., Armandroff, T. E., & Olszewski, E. W. 2002, *AJ*, 123, 2511
- Pierini, D. 2002, *MNRAS*, 330, 997
- Postman, M., & Geller, M. J. 1984, *ApJ*, 281, 95
- Prugniel, Ph., Bica, E., Klotz, A., & Alloin, D. 1993, *A&AS*, 98, 229
- Richer, M. G., & McCall, M. L. 1995, *ApJ*, 445, 642
- Salpeter, E. E. 1955, *ApJ*, 121, 161
- Sancisi, R., Thonnard, N., & Ekers, R. D. 1987, *ApJ*, 315, L39
- Sandage, A., Binggeli, B., & Tammann, G. A. 1985, *AJ*, 90, 1759
- Schlegel, D. J., Finkbeiner, D. P., & Davis, M. 1998, *ApJ*, 500, 525
- Sérsic, J.-L. 1968, *Atlas de galaxies australes*, Observatorio Astronomico, Cordoba
- Shetrone, M. D., Côté, P., Sargent, W. L. W. 2001, *ApJ*, 548, 592

- Shetrone, M., Venn, K. A., Tolstoy, E., Primas, F., Hill, V., & Kaufer, A. 2003, *AJ*, 125, 684
- Skillman, E. D. 1996, *ASP Conf. Ser.* 106: The Minnesota Lectures on Extragalactic Neutral Hydrogen, 208
- Skillman, E. D., Bothun, G. D., Murray, M. A., & Warmels, R. H. 1987, *A&A*, 185, 61
- Skillman, E. D., Kennicutt, R. C., & Hodge, P. W. 1989, *ApJ*, 347, 875
- Skillman, E. D., Tolstoy, E., Cole, A. A., Dolphin, A. E., Saha, A., Gallagher, J. S., Dohm-Palmer, R. C., & Mateo, M. 2003, *ApJ*, 596, 253
- Stoehr, F., White, S. D. M., Tormen, G., & Springel, V. 2002, *MNRAS*, 335, L84
- Thomas, D., Bender, R., Hopp, U., Maraston, C., & Greggio, L. 2003a, *Ap&SS*, 284, 599
- Thomas, D., Maraston, C., & Bender, R. 2003b, *MNRAS*, 339, 897
- Trager, S. C., Faber, S. M., Worthey, G., & González, J. J. 2000, *AJ*, 119, 1645
- Tully, R. B., & Pierce, M. J. 2000, *ApJ*, 533, 744
- Tully, R. B., & Shaya, E. J. 1984, *ApJ*, 281, 31
- Vader, J. P., Vigroux, L., Lachière-Rey, M., & Souviron, J. 1988, *A&A*, 203, 217
- van Zee, L. 2000 *AJ*, 119, 2757
- van Zee, L. 2001 *AJ*, 121, 2003
- van Zee, L., Haynes, M. P., & Giovanelli, R. 1995, *AJ*, 109, 990
- van Zee, L., Skillman, E. D., & Haynes, M. P. 2004, *AJ*, 128, 121
- Vigroux, L., Thuan, T. X., Vader, J. P., & Lachieze-Rey, M. 1986, *AJ*, 91, 70
- West, M. J., & Blakeslee, J. P. 2000, *ApJ*, 543, L27
- Worthey, G., & Ottaviani, D. L. 1997, *ApJS*, 111, 377
- Young, C. K., & Currie, M. J. 1995, *MNRAS*, 273, 1141

Table 1. Optical Imaging Observing Log

| Galaxy | Alternative Name | RA (2000) | Dec (2000) | Morph. Class. | VATT Filters ^a | Seeing | WIYN Filters | Seeing | notes |
|----------|------------------|------------|------------|---------------|---------------------------|--------|--------------|--------|-------|
| VCC 178 | IC 3081 | 12 16 09.1 | 12 41 28 | dE5,N | UBVRI | 1.3'' | BVRI | 1.2'' | b,c |
| VCC 437 | UGC 7399A | 12 20 48.8 | 17 29 13 | dE5,N | UBVRI | 1.7'' | BR | 0.7'' | b |
| VCC 543 | UGC 7436 | 12 22 19.5 | 14 45 39 | dE5 | UBVRI | 1.5'' | VRI | 1.4'' | |
| VCC 917 | IC 3344 | 12 26 32.4 | 13 34 43 | dE6 | BVRI | 2.1'' | BVRI | 1.2'' | |
| VCC 965 | IC 3363 | 12 27 02.9 | 12 33 37 | dE7,N | BVRI | 2.0'' | BVRI | 1.3'' | |
| VCC 990 | IC 3369 | 12 27 16.9 | 16 01 30 | dE4,N | UBVRI | 2.0'' | R | 1.8'' | d |
| VCC 1036 | NGC 4436 | 12 27 41.2 | 12 17 58 | dE6/dS0,N | UBVRI | 2.5'' | R | 1.4'' | |
| VCC 1075 | IC 3383 | 12 28 12.3 | 10 17 53 | dE4,N | BR | 1.5'' | | | |
| VCC 1122 | IC 3393 | 12 28 41.7 | 12 54 57 | dE7,N | UBVRI | 2.0'' | BVRI | 1.1'' | e |
| VCC 1261 | NGC 4482 | 12 30 10.3 | 10 46 47 | dE,N | BVRI | 2.5'' | R | 1.5'' | |
| VCC 1308 | IC 3437 | 12 30 45.9 | 11 20 37 | dE,N | BVRI | 1.9'' | R | 1.2'' | |
| VCC 1514 | CGCG 042-152 | 12 33 37.7 | 07 52 19 | dE7,N | UBVRI | 2.4'' | R | 1.1'' | |
| VCC 1743 | IC 3602 | 12 38 06.8 | 10 04 57 | dE6 | BR | 1.1'' | | | |
| VCC 1857 | IC 3647 | 12 40 53.1 | 10 28 34 | dE | BR | 1.4'' | | | |
| VCC 2019 | IC 3735 | 12 45 20.4 | 13 41 35 | E? | UBVRI | 2.4'' | R | 1.6'' | f |
| VCC 2050 | IC 3779 | 12 47 20.7 | 12 09 59 | dE5;N | UBVRI | 1.9'' | R | 1.3'' | |

Note. — Morphological classification from Binggeli et al. (1985).

^aUnless otherwise noted, VATT integration times were sets of 2×540 sec, 2×420 sec, 2×300 sec, 2×240 sec, and 2×300 sec for UBVR, respectively.

^bR = 2×300 s; B = 2×600 s.

^cV = 2×240 s.

^dU = 3×540 s.

^eU = 1×540 s.

^fR = 2×420 s.

Table 2. Observed Properties of dE Sample

| Galaxy | R_{25} [arcsec] | PA | ellipticity | inc. | m_B | A_B | (U-B) | (B-V) | (B-R) | (V-I) | Non-elliptical Isophotes? | Rot. Curve Slope [km s ⁻¹ kpc ⁻¹] |
|----------|----------------------|-------------|-------------|------|--------------|-------|-------------|-------------|-------------|-------------|------------------------------|---|
| VCC 178 | 22.3 | 86.4 ± 0.5 | 0.42 ± 0.01 | 54 | 15.81 ± 0.04 | 0.150 | 0.28 ± 0.05 | 0.81 ± 0.08 | 1.33 ± 0.04 | 1.06 ± 0.03 | Y | 22.7 ± 2.6 |
| VCC 437 | 48.8 | 76.3 ± 2.6 | 0.35 ± 0.09 | 49 | 14.38 ± 0.04 | 0.133 | 0.31 ± 0.05 | 0.82 ± 0.07 | 1.36 ± 0.04 | 1.09 ± 0.03 | Y | 25.0 ± 3.1 |
| VCC 543 | 42.4 | 120.4 ± 3.1 | 0.44 ± 0.03 | 56 | 14.58 ± 0.05 | 0.136 | 0.30 ± 0.05 | 0.81 ± 0.07 | 1.35 ± 0.04 | 1.09 ± 0.03 | N | 25.4 ± 2.2 |
| VCC 917 | 24.8 | 57.9 ± 1.1 | 0.44 ± 0.06 | 56 | 15.68 ± 0.03 | 0.139 | ... | 0.77 ± 0.07 | 1.29 ± 0.04 | 1.03 ± 0.03 | Y | 10.4 ± 4.9 |
| VCC 965 | 32.0 | 125.5 ± 1.6 | 0.49 ± 0.08 | 59 | 15.72 ± 0.04 | 0.130 | ... | 0.78 ± 0.07 | 1.30 ± 0.04 | 1.02 ± 0.03 | Y | 25.1 ± 3.6 |
| VCC 990 | 26.1 | 135.0 ± 0.9 | 0.30 ± 0.04 | 46 | 14.85 ± 0.05 | 0.121 | 0.26 ± 0.05 | 0.82 ± 0.07 | 1.34 ± 0.04 | 1.07 ± 0.03 | Y | 26.3 ± 2.2 |
| VCC 1036 | 52.9 | 112.9 ± 0.4 | 0.52 ± 0.05 | 61 | 14.18 ± 0.03 | 0.119 | 0.31 ± 0.05 | 0.83 ± 0.07 | 1.36 ± 0.04 | 1.12 ± 0.03 | Y | 23.1 ± 1.0 |
| VCC 1075 | 26.6 | 26.6 ± 1.1 | 0.32 ± 0.02 | 47 | 15.34 ± 0.05 | 0.116 | ... | ... | 1.32 ± 0.04 | ... | N | ... |
| VCC 1122 | 36.0 | 132.5 ± 0.4 | 0.53 ± 0.06 | 62 | 15.09 ± 0.04 | 0.091 | 0.21 ± 0.05 | 0.77 ± 0.07 | 1.28 ± 0.04 | 1.02 ± 0.03 | Y | 18.1 ± 2.3 |
| VCC 1261 | 51.8 | 134.4 ± 1.0 | 0.37 ± 0.06 | 51 | 13.78 ± 0.04 | 0.122 | ... | 0.80 ± 0.07 | 1.32 ± 0.04 | 1.08 ± 0.04 | N | 0.90 ± 1.5 |
| VCC 1308 | 22.4 | 66.1 ± 0.8 | 0.32 ± 0.06 | 47 | 15.83 ± 0.04 | 0.151 | ... | 0.81 ± 0.08 | 1.32 ± 0.05 | 1.05 ± 0.04 | N | 12.0 ± 3.8 |
| VCC 1514 | 36.8 | 6.6 ± 1.2 | 0.65 ± 0.03 | 70 | 15.59 ± 0.04 | 0.084 | 0.26 ± 0.06 | 0.76 ± 0.09 | 1.24 ± 0.05 | 1.03 ± 0.04 | Y | 12.0 ± 2.4 |
| VCC 1743 | 25.6 | 130.8 ± 0.4 | 0.55 ± 0.02 | 63 | 15.92 ± 0.04 | 0.085 | ... | ... | 1.30 ± 0.05 | ... | Y | 40.9 ± 24.1 |
| VCC 1857 | 36.6 | 135.9 ± 4.9 | 0.55 ± 0.04 | 63 | 15.34 ± 0.05 | 0.112 | ... | ... | 1.17 ± 0.04 | ... | Y | 26.2 ± 7.2 |
| VCC 2019 | 30.3 | 151.6 ± 6.3 | 0.27 ± 0.03 | 43 | 14.78 ± 0.04 | 0.094 | 0.25 ± 0.05 | 0.84 ± 0.08 | 1.34 ± 0.05 | 1.04 ± 0.04 | N | 28.3 ± 2.8 |
| VCC 2050 | 25.9 | 125.9 ± 0.8 | 0.48 ± 0.02 | 59 | 15.62 ± 0.04 | 0.100 | 0.22 ± 0.05 | 0.80 ± 0.08 | 1.31 ± 0.03 | 1.06 ± 0.05 | Y | 16.7 ± 2.6 |

Note. — R_{25} is the radius at which μ_B equals 25 mag arcsec⁻². Position Angle and ellipticity are the mean values for radii between 5'' and R_{25} . m_B is the magnitude at which the curve of growth levels off. The Galactic Extinction, A_B , is tabulated from NED, based on the extinction models of Schlegel et al. (1998). (U-B), (B-V), (B-R), and (V-I) are measured within the R_{25} aperture. The second-to-last column indicates if there were significant residuals in the image after subtracting off the best fit ellipses. The final column lists the slope of the rotation curve as measured in van Zee et al. (2004). Galaxies with rotation curve slopes greater than 20 km s⁻¹ kpc⁻¹ have significant rotation.

Table 3. Derived Properties of dE Sample

| Galaxy | M_B | $\mu_{B,eff}$ | R_{eff} [arcsec, (kpc)] | μ_B^0 | $\mu_B^{0,c}$ | α [arcsec, (kpc)] | $\mu_{R,s}$ | r_s [arcsec] | n | (U-B) ₀ | (B-V) ₀ | (B-R) ₀ | (V-I) ₀ |
|----------|--------|---------------|------------------------------|-----------|---------------|-----------------------------|--------------|-------------------|-------------|--------------------|--------------------|--------------------|--------------------|
| VCC 178 | -15.37 | 22.53 | 8.7 (0.68) | 21.39 | 21.97 | 6.7 (0.52) | 19.85 ± 0.03 | 4.06 ± 0.12 | 0.87 ± 0.01 | 0.24 ± 0.05 | 0.77 ± 0.08 | 1.27 ± 0.04 | 1.01 ± 0.03 |
| VCC 437 | -16.79 | 23.10 | 22.1 (1.73) | 22.41 | 22.86 | 20.4 (1.60) | 19.10 ± 0.04 | 2.34 ± 0.14 | 0.52 ± 0.01 | 0.28 ± 0.05 | 0.79 ± 0.07 | 1.31 ± 0.04 | 1.05 ± 0.03 |
| VCC 543 | -16.59 | 22.83 | 17.9 (1.40) | 22.07 | 22.70 | 15.8 (1.23) | 18.82 ± 0.04 | 1.94 ± 0.12 | 0.54 ± 0.01 | 0.26 ± 0.05 | 0.78 ± 0.07 | 1.30 ± 0.04 | 1.05 ± 0.03 |
| VCC 917 | -15.49 | 22.13 | 7.8 (0.61) | 21.53 | 22.17 | 7.8 (0.60) | 19.02 ± 0.04 | 2.36 ± 0.11 | 0.74 ± 0.01 | ... | 0.73 ± 0.07 | 1.24 ± 0.04 | 0.99 ± 0.03 |
| VCC 965 | -15.44 | 23.41 | 13.8 (1.08) | 22.44 | 23.16 | 13.6 (1.06) | 20.94 ± 0.03 | 7.79 ± 0.22 | 0.93 ± 0.02 | ... | 0.75 ± 0.07 | 1.25 ± 0.04 | 0.98 ± 0.03 |
| VCC 990 | -16.31 | 21.77 | 9.7 (0.75) | 20.81 | 21.20 | 6.8 (0.53) | 17.88 ± 0.06 | 1.38 ± 0.08 | 0.58 ± 0.01 | 0.23 ± 0.05 | 0.79 ± 0.07 | 1.29 ± 0.04 | 1.03 ± 0.03 |
| VCC 1036 | -16.97 | 21.99 | 14.6 (1.14) | 21.59 | 22.38 | 16.9 (1.32) | 17.69 ± 0.06 | 1.06 ± 0.08 | 0.49 ± 0.01 | 0.28 ± 0.05 | 0.80 ± 0.07 | 1.32 ± 0.04 | 1.08 ± 0.03 |
| VCC 1075 | -15.81 | 23.33 | 15.8 (1.23) | 21.93 | 22.34 | 9.4 (0.73) | 20.06 ± 0.04 | 3.92 ± 0.20 | 0.67 ± 0.01 | ... | ... | 1.28 ± 0.04 | ... |
| VCC 1122 | -16.03 | 22.37 | 11.4 (0.89) | 21.61 | 22.43 | 11.5 (0.90) | 19.18 ± 0.04 | 2.96 ± 0.13 | 0.70 ± 0.01 | 0.19 ± 0.05 | 0.75 ± 0.07 | 1.24 ± 0.04 | 0.99 ± 0.03 |
| VCC 1261 | -17.38 | 22.21 | 19.4 (1.51) | 21.22 | 21.72 | 14.9 (1.16) | 18.30 ± 0.04 | 2.26 ± 0.13 | 0.55 ± 0.01 | ... | 0.77 ± 0.07 | 1.27 ± 0.04 | 1.04 ± 0.03 |
| VCC 1308 | -15.36 | 22.62 | 9.1 (0.71) | 21.62 | 22.03 | 7.2 (0.56) | 19.52 ± 0.05 | 2.69 ± 0.15 | 0.71 ± 0.01 | ... | 0.77 ± 0.08 | 1.26 ± 0.05 | 1.00 ± 0.03 |
| VCC 1514 | -15.53 | 23.26 | 13.7 (1.07) | 22.11 | 23.28 | 13.5 (1.05) | 20.76 ± 0.03 | 7.04 ± 0.25 | 0.88 ± 0.02 | 0.24 ± 0.06 | 0.74 ± 0.09 | 1.21 ± 0.05 | 1.00 ± 0.03 |
| VCC 1743 | -15.20 | 23.05 | 10.7 (0.83) | 21.78 | 22.64 | 8.6 (0.67) | 20.02 ± 0.05 | 3.35 ± 0.20 | 0.71 ± 0.02 | ... | ... | 1.27 ± 0.05 | ... |
| VCC 1857 | -15.81 | 23.75 | 19.2 (1.50) | 22.41 | 23.27 | 15.4 (1.20) | 21.85 ± 0.01 | 16.96 ± 0.27 | 1.24 ± 0.02 | ... | ... | 1.13 ± 0.04 | ... |
| VCC 2019 | -16.34 | 22.84 | 16.3 (1.28) | 21.46 | 21.80 | 9.3 (0.73) | 19.41 ± 0.05 | 3.19 ± 0.20 | 0.62 ± 0.01 | 0.23 ± 0.05 | 0.82 ± 0.08 | 1.30 ± 0.05 | 1.01 ± 0.03 |
| VCC 2050 | -15.51 | 22.72 | 10.5 (0.82) | 21.59 | 22.21 | 8.0 (0.62) | 19.76 ± 0.04 | 3.57 ± 0.16 | 0.74 ± 0.01 | 0.19 ± 0.05 | 0.78 ± 0.08 | 1.27 ± 0.03 | 1.03 ± 0.03 |

Note. — M_B has been corrected for Galactic extinction and assumes a distance modulus of 31.03. The effective surface brightness and effective radius, $\mu_{B,eff}$ and R_{eff} , are calculated from the B-band image; the effective radius is the geometric mean radius, \sqrt{ab} , at half-light of the apparent B-band magnitude. The disk-like parameters μ_B^0 and α are derived from exponential fits to the outer regions of the galaxies; here, the radius is defined as the semi-major axis and $\mu_B^{0,c}$ has been corrected for both inclination and Galactic extinction. Sérsic fits to the R-band surface brightness profiles are parameterized by $\mu_{R,s}$, r_s , and n; the fits have been scaled for the geometric mean radii. The listed colors are corrected for Galactic extinction.

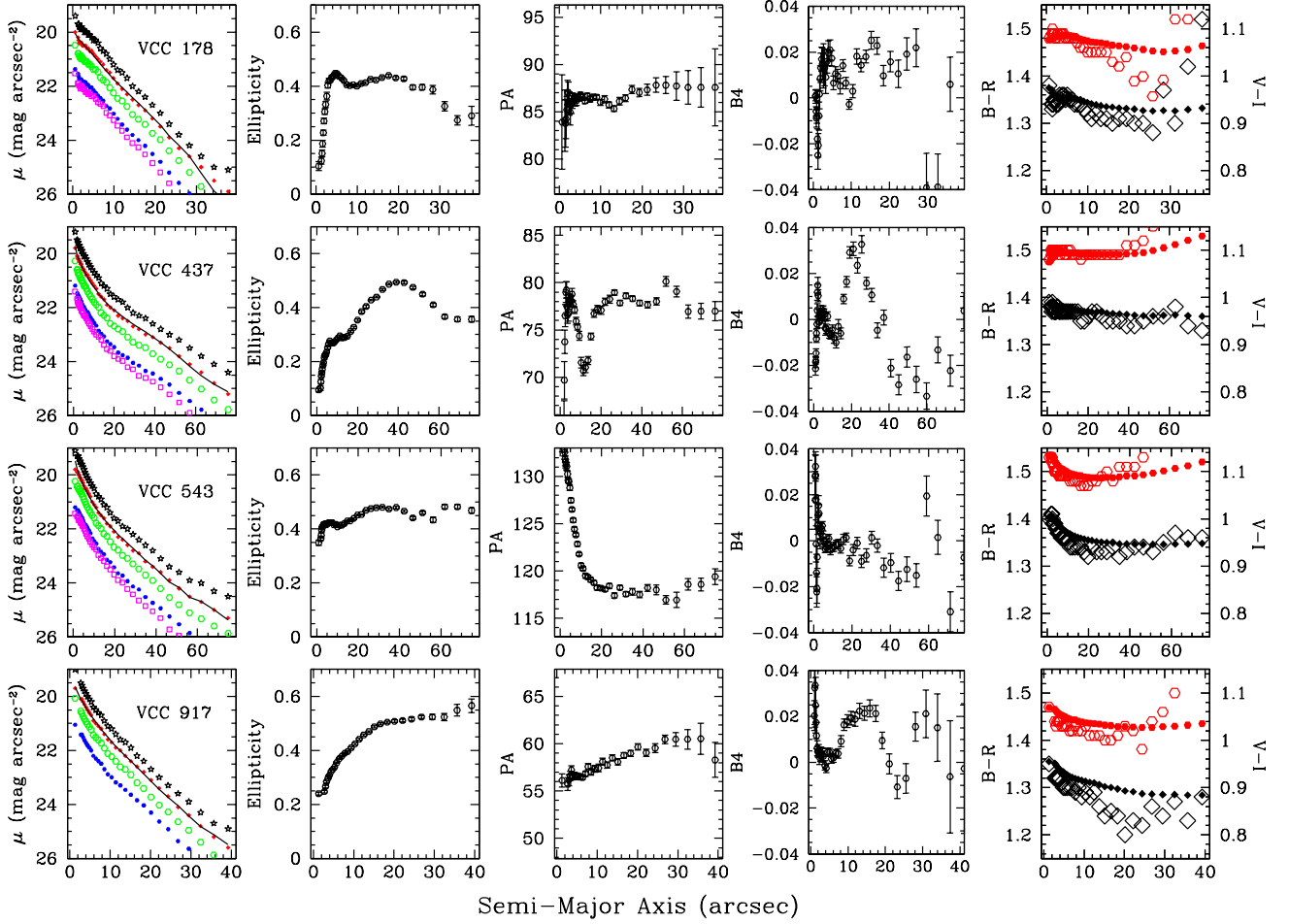
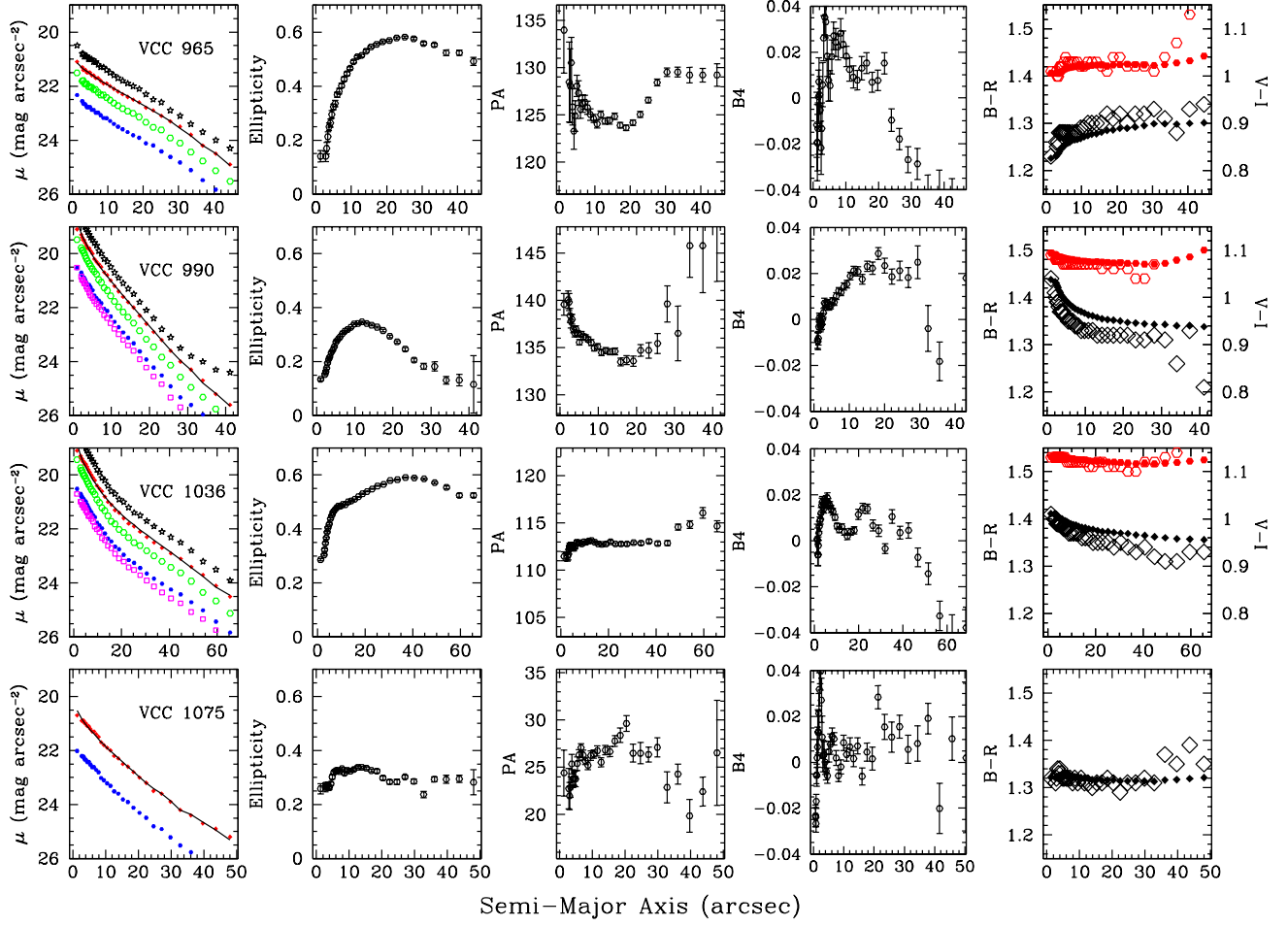
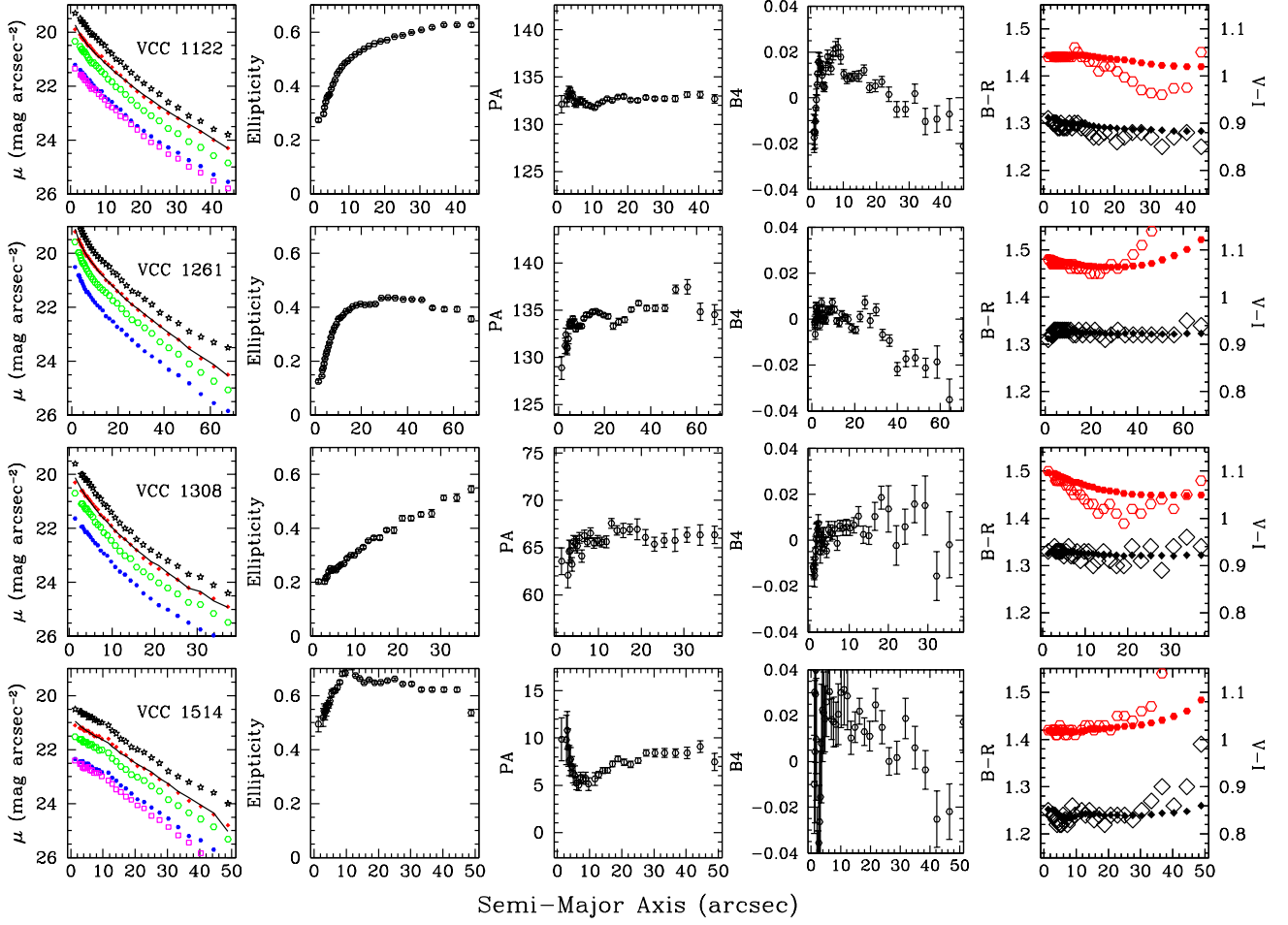
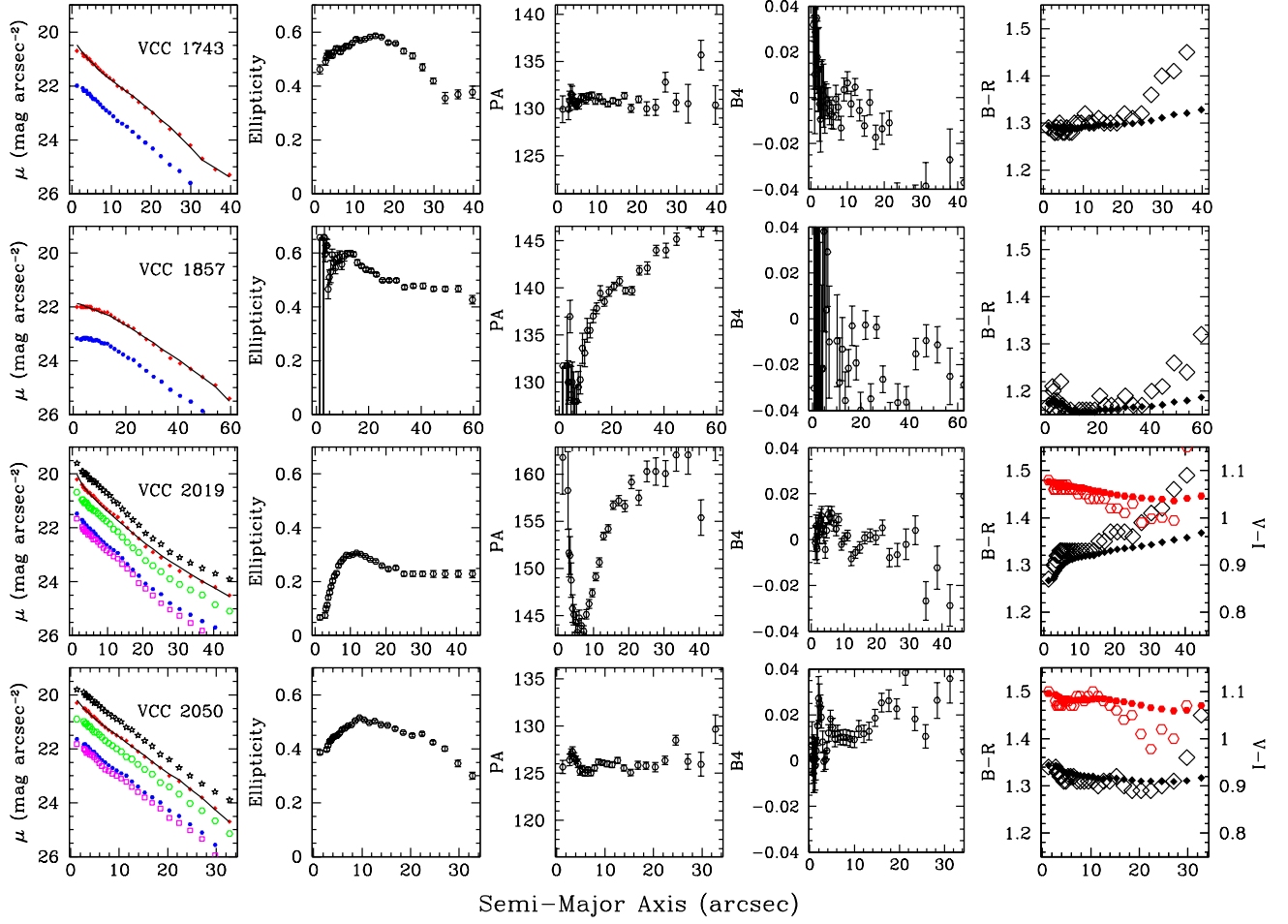


Fig. 1.— Surface photometry for 16 dwarf elliptical galaxies. The left-most panels show the surface brightness as a function of radius for U (open squares), B (filled hexagons), V (open hexagons), R (filled diamonds), and I (stars). The middle panels show the ellipticity, position angle, and B4 as a function of radius for the ELLIPSE fits to the R-band images. The right-most panels show the observed B-R color (black diamonds) and V-I color (red hexagons) for each elliptical annulus (open symbols) and for the integrated light within that aperture (filled symbols).







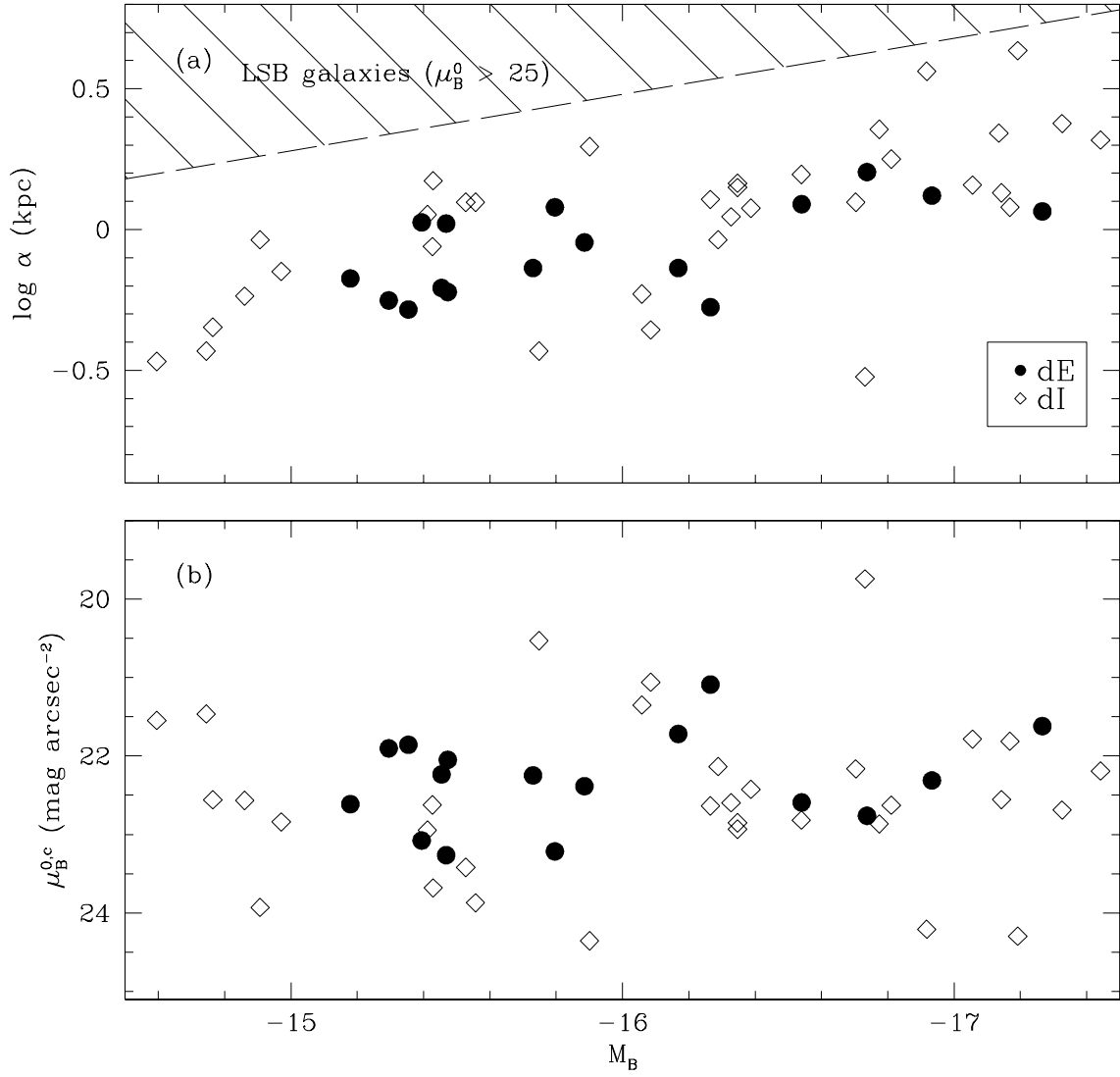


Fig. 2.— Structural parameters for exponential fits to dwarf elliptical (filled symbols) and dwarf irregular (open symbols; van Zee 2001) galaxies. (a) Scale length as function of absolute magnitude. (b) Surface brightness as function of absolute magnitude. The dwarf elliptical and dwarf irregular galaxies share a common locus in these diagrams.

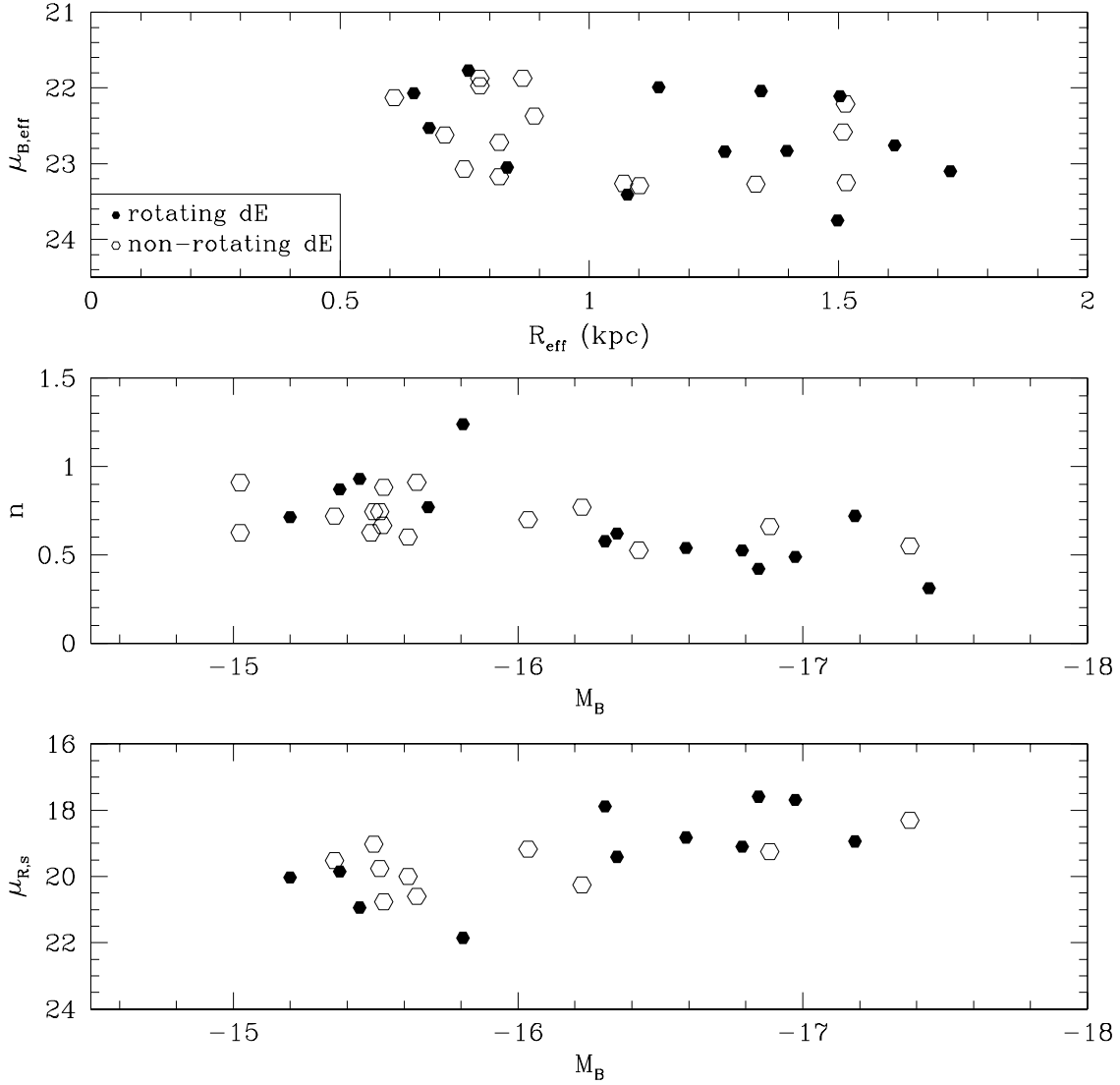


Fig. 3.— Structural parameters for Sérsic fits to dwarf elliptical galaxies in Virgo with measured kinematic properties (Pedraz et al. 2002; Geha et al. 2003; the present sample); rotating (filled hexagons) and non-rotating (open hexagons) dE galaxies have similar structural properties. (a) Model independent parameters of half-light radius and effective surface brightness. (b) Absolute magnitude and Sérsic shape parameter. (c) Absolute magnitude and central surface brightness from a Sérsic fit to the R-band surface brightness profile. The non-rotating and rotating dwarf elliptical galaxies cannot be distinguished based on structural parameters.

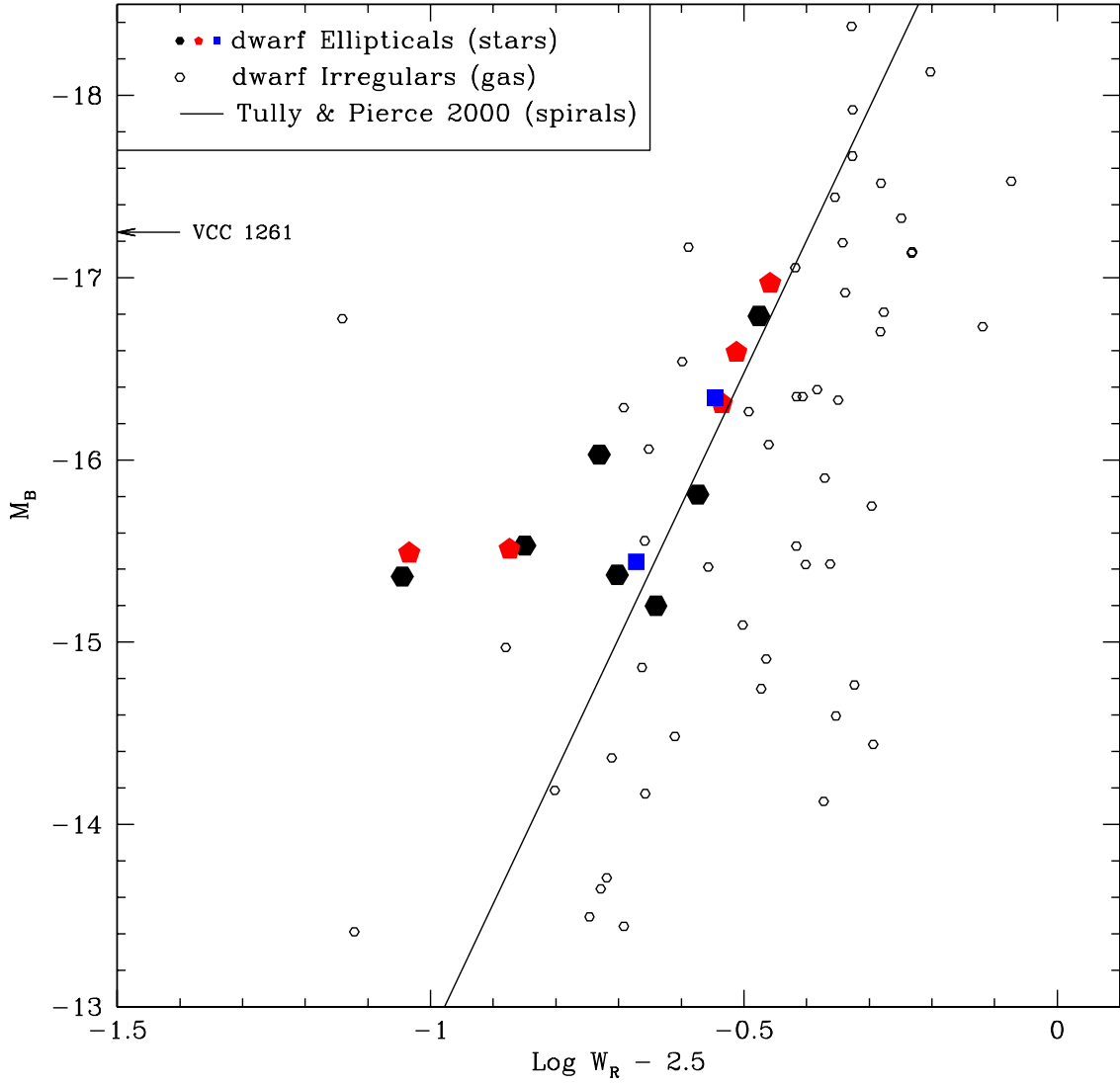


Fig. 4.— The luminosity-line width relation for dwarf elliptical galaxies [note that the values shown are the observed maximum linewidths, which are possible underestimates of the full rotation velocity; see van Zee et al. (2004) for a full discussion of possible correction factors to the observed widths]. Dwarf ellipticals with blue cores (blue squares) and red cores (red pentagons) follow the same relation as spiral galaxies (line; Tully & Pierce 2000) and dwarf irregular galaxies (open dots; van Zee 2001).

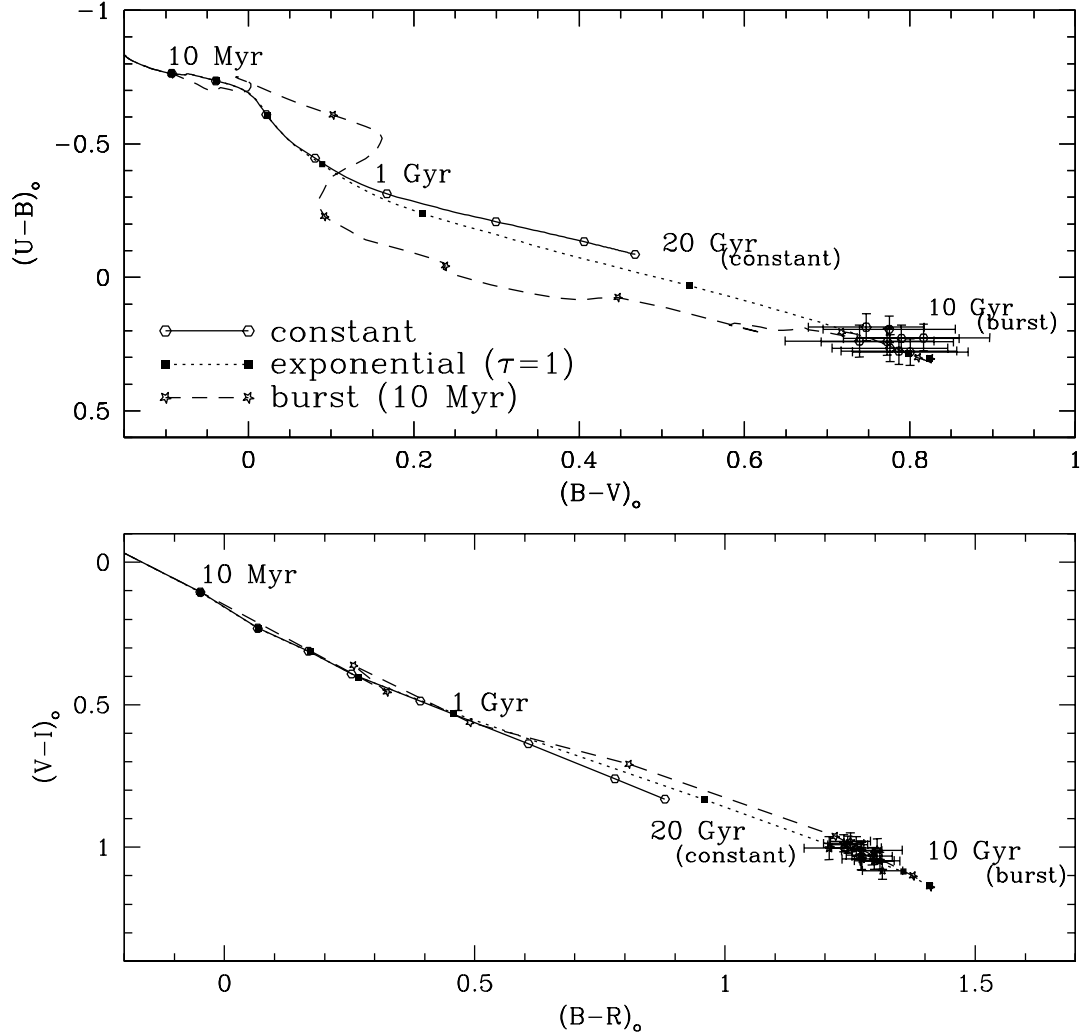


Fig. 5.— Optical colors of dwarf elliptical galaxies in the Virgo Cluster. Three fiducial evolutionary tracks are shown for low metallicity (1/5 solar) composite stellar populations from the Bruzual & Charlot (2003) models. The models include a short (10 Myr) burst of star formation (long dashed lines), an exponentially decreasing star formation rate, with and e-folding time of 1 Gyr (short dashed lines), and a constant star formation rate (solid lines). The models are marked every 0.5 dex, and time increases from the upper left hand corner to the lower right hand corner. The short burst and exponentially decreasing star formation rates both result in a red galaxy after a Hubble time, while a constant star formation rate results in a blue system. The three star formation histories can be separated in the UBV color-color diagram but all three models are degenerate in the color-color space of $(B-R)$ vs. $(V-I)$. The observed colors are consistent with an evolved stellar population with an age of approximately 6 Gyr.

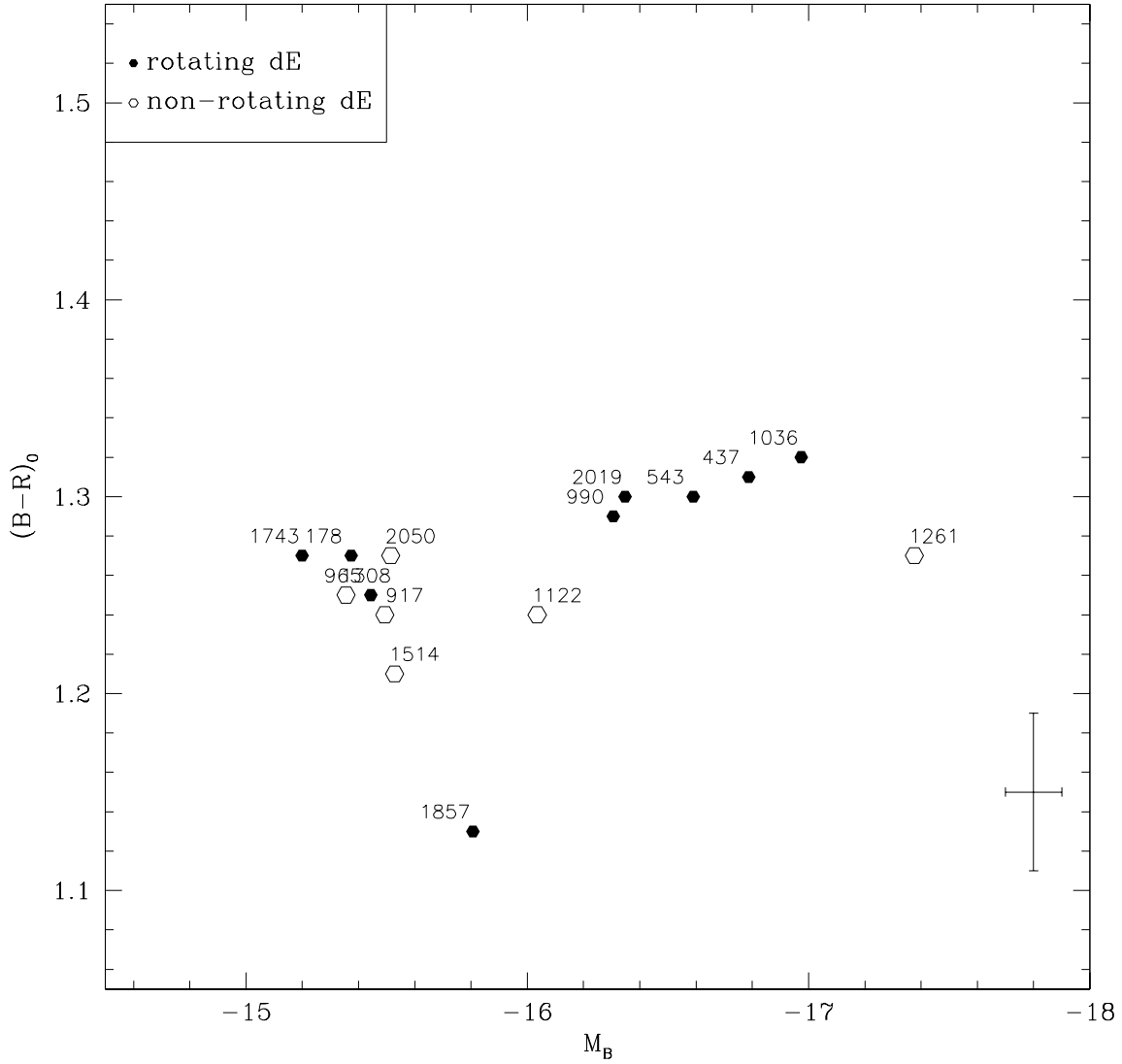


Fig. 6.— Color-magnitude diagram for dwarf elliptical galaxies with measured kinematic properties. The more luminous dEs are slightly redder than the lower luminosity galaxies, indicating a change in age or metallicity of the dominant stellar population. The two significant outliers in this diagram are VCC 1857 and VCC 1261, one of which appears to be rotationally supported while the other has no evidence of rotation (kinematics from major-axis spectroscopy only). These observations indicate that there are no clear differences in the optical colors of rotating (filled hexagons) and non-rotating (open hexagons) dwarf elliptical galaxies.

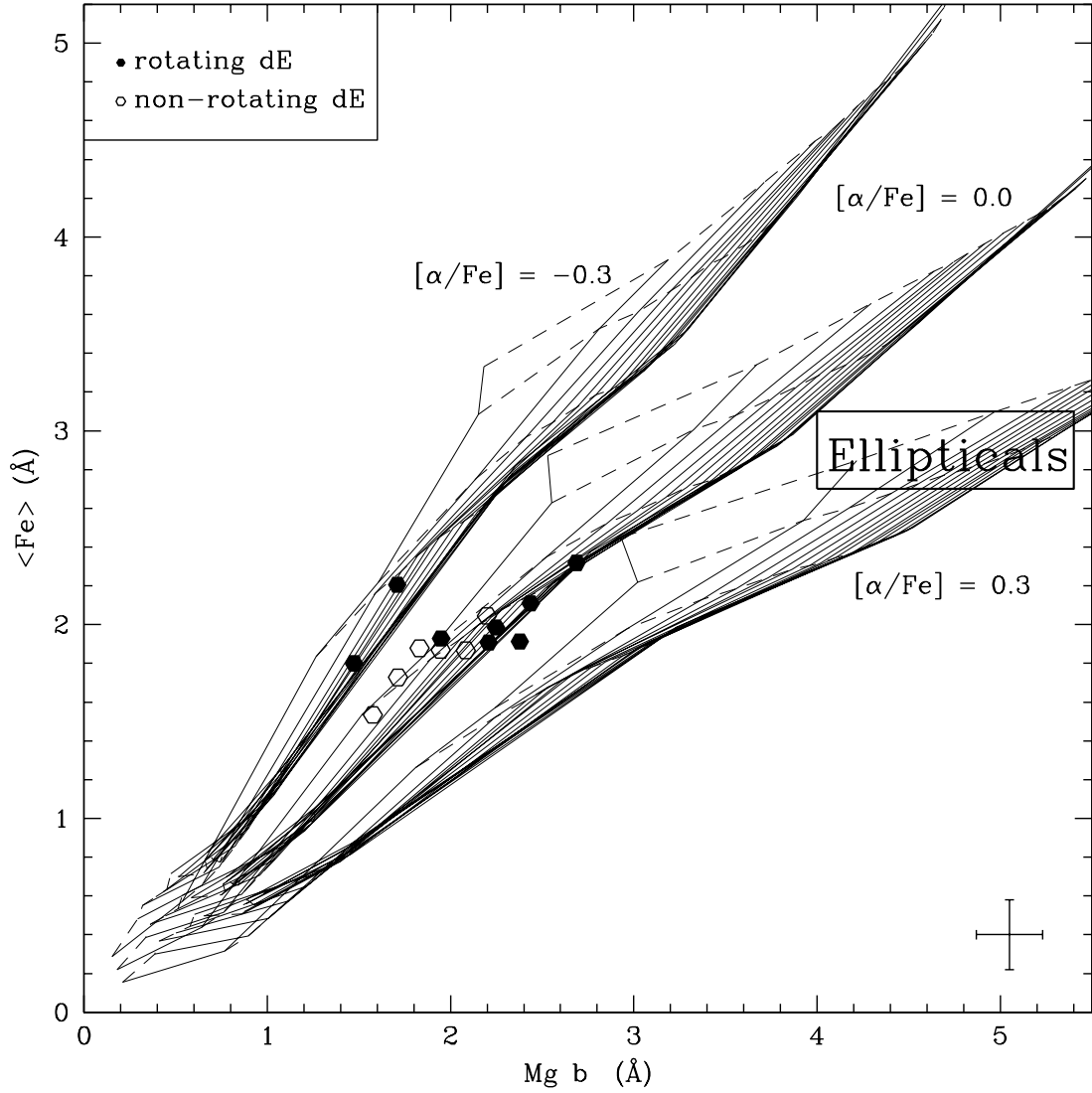


Fig. 7.— Mgb and $\langle Fe \rangle$ Lick/IDS indices for Virgo dwarf elliptical galaxies. The locus for giant elliptical galaxies from Trager et al. (2000) is also shown. The stellar population models of Thomas et al. (2003b) are shown for several ages ($t = 1$ to 15 Gyr in 1 Gyr increments) and for several $[\alpha/\text{Fe}]$ models ($[\alpha/\text{Fe}] = -0.3, 0.0,$ and 0.3 dex). The majority of dwarf elliptical galaxies are well fit by models with solar $[\alpha/\text{Fe}]$ ratios.

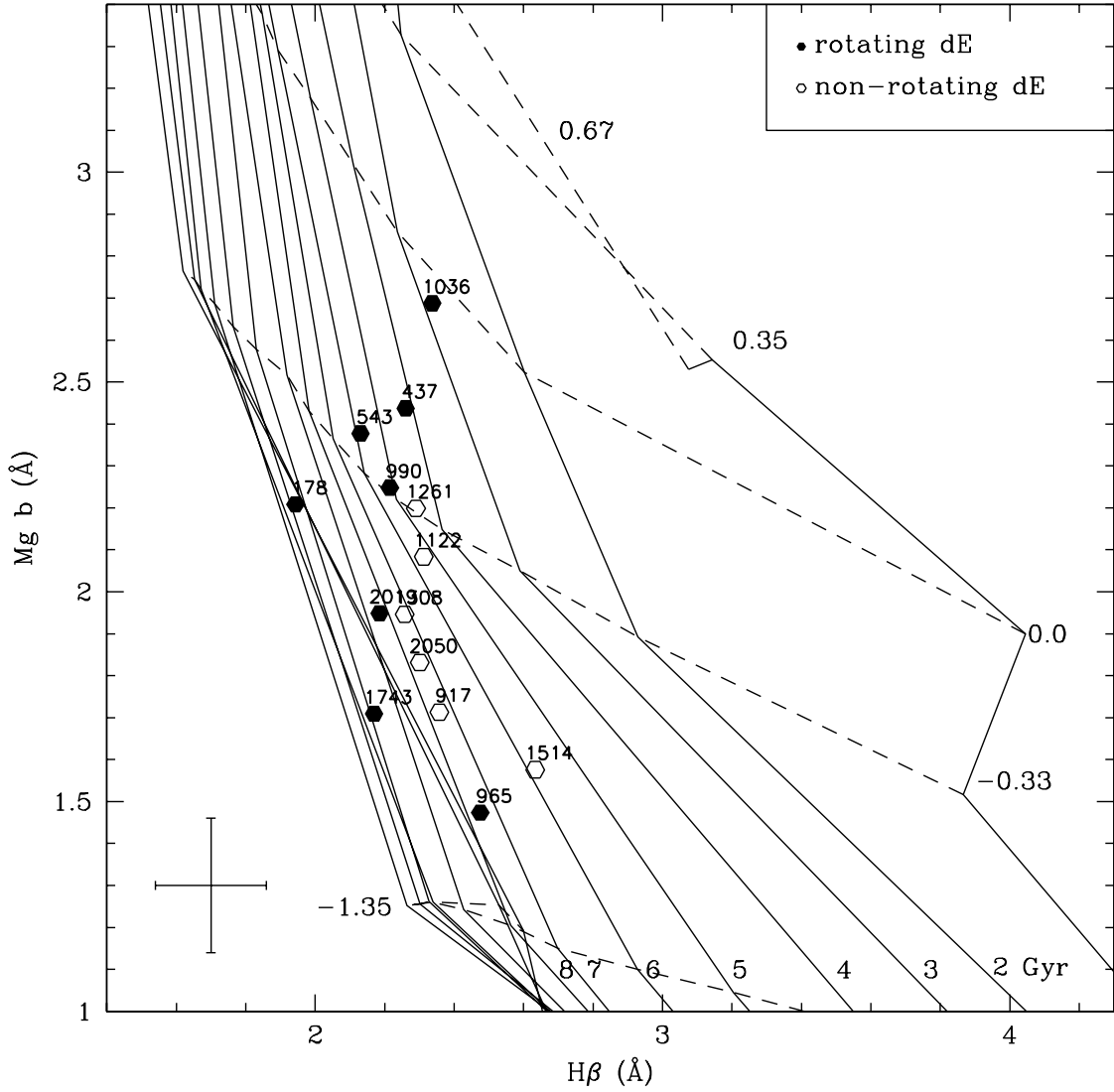


Fig. 8.— Mgb and H β Lick/IDS indices for Virgo dwarf elliptical galaxies. Stellar population models with solar $[\alpha/\text{Fe}]$ ratios (Thomas et al. 2003b) are shown for several metallicities ($[\text{Fe}/\text{H}] = -0.33, 0.0, 0.33, \text{ and } 0.67$ dex) and for several ages ($t = 1$ to 15 Gyr in 1 Gyr increments). The majority of dwarf elliptical galaxies contain low metallicity ($[\text{Fe}/\text{H}] < -0.33$) evolved stellar populations ($t \sim 5\text{-}7$ Gyr).